Article

Cell Stem Cell

Cardiac Fibroblasts Adopt Osteogenic Fates and Can Be Targeted to Attenuate Pathological Heart Calcification

Graphical Abstract

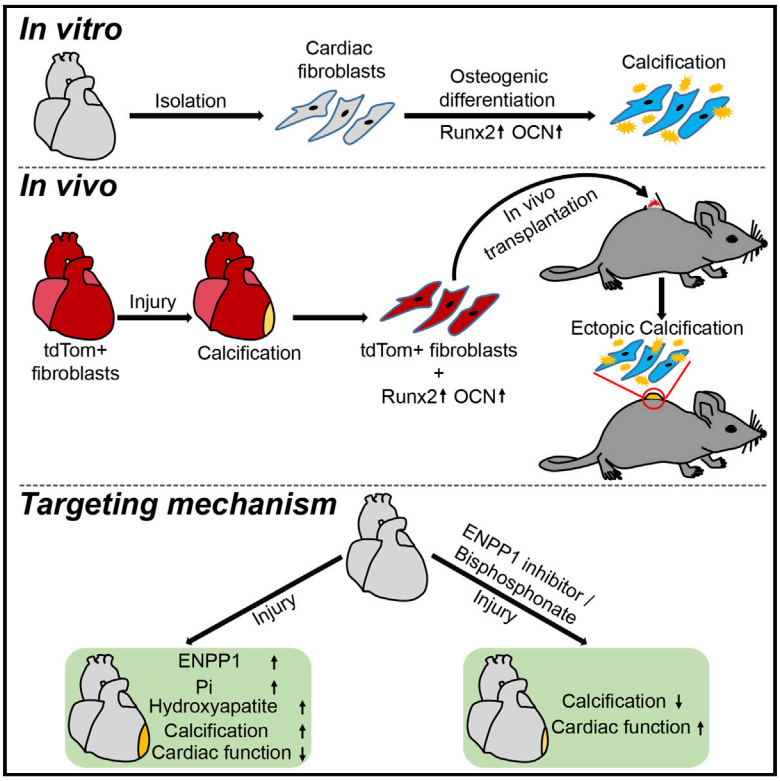

Authors

Indulekha C.L. Pillai, Shen Li, Milagros Romay, ..., Matteo Pellegrini, Aldons J. Lusis, Arjun Deb

Correspondence

adeb@mednet.ucla.edu

In Brief

Pillai et al. demonstrate that cardiac fibroblasts adopt bone-forming cell fates and induce ectopic calcification. ENPP1, an enzyme that regulates bone mineralization, is induced in cardiac fibroblasts after injury. Administration of ENPP1 inhibitors or inhibitors of bone mineralization significantly decreased pathologic cardiac calcification and augmented cardiac function.

Highlights

- CFs express osteogenic markers in vitro and in several murine heart calcification models
- CFs from calcified hearts can induce ectopic calcification upon transplantation
- CFs induce mineralization of the matrix via upregulation of ENPP1
- Inhibitors of ENPP1 and mineralization decrease calcification and improve cardiac function

Data Resources

GSE87836
GSE87837

Pillai et al., 2017, Cell Stem Cell *20*, 218–232
February 2, 2017
http://dx.doi.org/10.1016/j.stem.2016.10.005

CellPress

Cell Stem Cell
Article

Cardiac Fibroblasts Adopt Osteogenic Fates and Can Be Targeted to Attenuate Pathological Heart Calcification

Indulekha C.L. Pillai,[1,2,3,4,5,6,12] Shen Li,[1,2,3,4,5,6,12] Milagros Romay,[2,7] Larry Lam,[3,4,5,6] Yan Lu,[1,2,3,4,5,6] Jie Huang,[1,2,3,4,5,6] Nathaniel Dillard,[1,2,3,4,5,6] Marketa Zemanova,[1,2,3,4,5,6] Liudmilla Rubbi,[3,4,5,6] Yibin Wang,[2,8,9] Jason Lee,[6,10] Ming Xia,[6,11] Owen Liang,[6,11] Ya-Hong Xie,[6,11] Matteo Pellegrini,[3,4,5,6] Aldons J. Lusis,[1,2,7] and Arjun Deb[1,2,3,4,5,6,13,*]

[1]Division of Cardiology, Department of Medicine, David Geffen School of Medicine, University of California, Los Angeles (UCLA), CA 90095, USA
[2]Cardiovascular Research Laboratory, David Geffen School of Medicine, UCLA, CA 90095, USA
[3]Department of Molecular, Cell and Developmental Biology, School of Letters and Sciences, UCLA, CA 90095, USA
[4]Eli & Edythe Broad Center of Regenerative Medicine and Stem Cell Research, UCLA, CA 90095, USA
[5]Molecular Biology Institute, UCLA, CA 90095, USA
[6]Jonsson Comprehensive Cancer Center, UCLA, CA 90095, USA
[7]Departments of Human Genetics & Microbiology, Immunology, and Molecular Genetics, UCLA, CA 90095, USA
[8]Department of Anesthesiology, UCLA, CA 90095, USA
[9]Department of Physiology, UCLA, CA 90095, USA
[10]Department of Molecular and Medical Pharmacology, David Geffen School of Medicine and Crump Institute for Molecular Imaging, UCLA, CA 90095, USA
[11]Department of Materials Science & Engineering, School of Engineering, UCLA, CA 90095, USA
[12]Co-first author
[13]Lead Contact
*Correspondence: adeb@mednet.ucla.edu
http://dx.doi.org/10.1016/j.stem.2016.10.005

SUMMARY

Mammalian tissues calcify with age and injury. Analogous to bone formation, osteogenic cells are thought to be recruited to the affected tissue and induce mineralization. In the heart, calcification of cardiac muscle leads to conduction system disturbances and is one of the most common pathologies underlying heart blocks. However the cell identity and mechanisms contributing to pathological heart muscle calcification remain unknown. Using lineage tracing, murine models of heart calcification and in vivo transplantation assays, we show that cardiac fibroblasts (CFs) adopt an osteoblast cell-like fate and contribute directly to heart muscle calcification. Small-molecule inhibition of ENPP1, an enzyme that is induced upon injury and regulates bone mineralization, significantly attenuated cardiac calcification. Inhibitors of bone mineralization completely prevented ectopic cardiac calcification and improved post injury heart function. Taken together, these findings highlight the plasticity of fibroblasts in contributing to ectopic calcification and identify pharmacological targets for therapeutic development.

INTRODUCTION

Pathological mineralization of soft tissues, or ectopic calcification, commonly occurs with tissue injury and degeneration and in common diseases such as diabetes and chronic kidney disease. Calcification of soft tissues is a cell mediated process that resembles bone formation in the skeletal system with calcification of the extracellular matrix by cells capable of mineralization (Demer and Tintut, 2014). Heart muscle calcification is an under-reported and unusual form of soft tissue calcification characterized by calcific deposits within the myocardium, which can occur in the absence of calcification of valves, vessels, or other organs (Shackley et al., 2011). Myocardial calcification is observed in the aging heart and in patients with diabetes, renal disease, and myocardial injury secondary to ischemia or inflammation (Rostand et al., 1988). Calcification within the heart muscle is one of the most common underlying causes of heart blocks where calcification and fibrosis of the conduction system interrupt smooth propagation of electrical impulses (Lev, 1964). Cardiac pump dysfunction and arrhythmias can also occur depending on the extent and anatomic site of calcification and calcified myocardial scars have been reported to cause refractory ventricular tachycardia. Cardiac calcification is also a prognostic indicator of poor outcomes following myocardial infarction or myocarditis (Stallion et al., 1994). Even during embryonic development, progressive calcification of myocardial walls can occur and leads to fetal or neonatal demise (Simchen et al., 2006).

Despite the occurrence of heart muscle calcification in a variety of disease conditions, little is known about the identity of cells contributing to pathological myocardial calcification. We have recently demonstrated that cardiac fibroblasts (CFs) can exhibit plasticity after heart injury and adopt alternative cell fates (Ubil et al., 2014). Ectopic calcification of soft tissues usually occurs in areas of injury associated with fibrosis (Pugashetti et al., 2011) and this led us to hypothesize that CFs can adopt

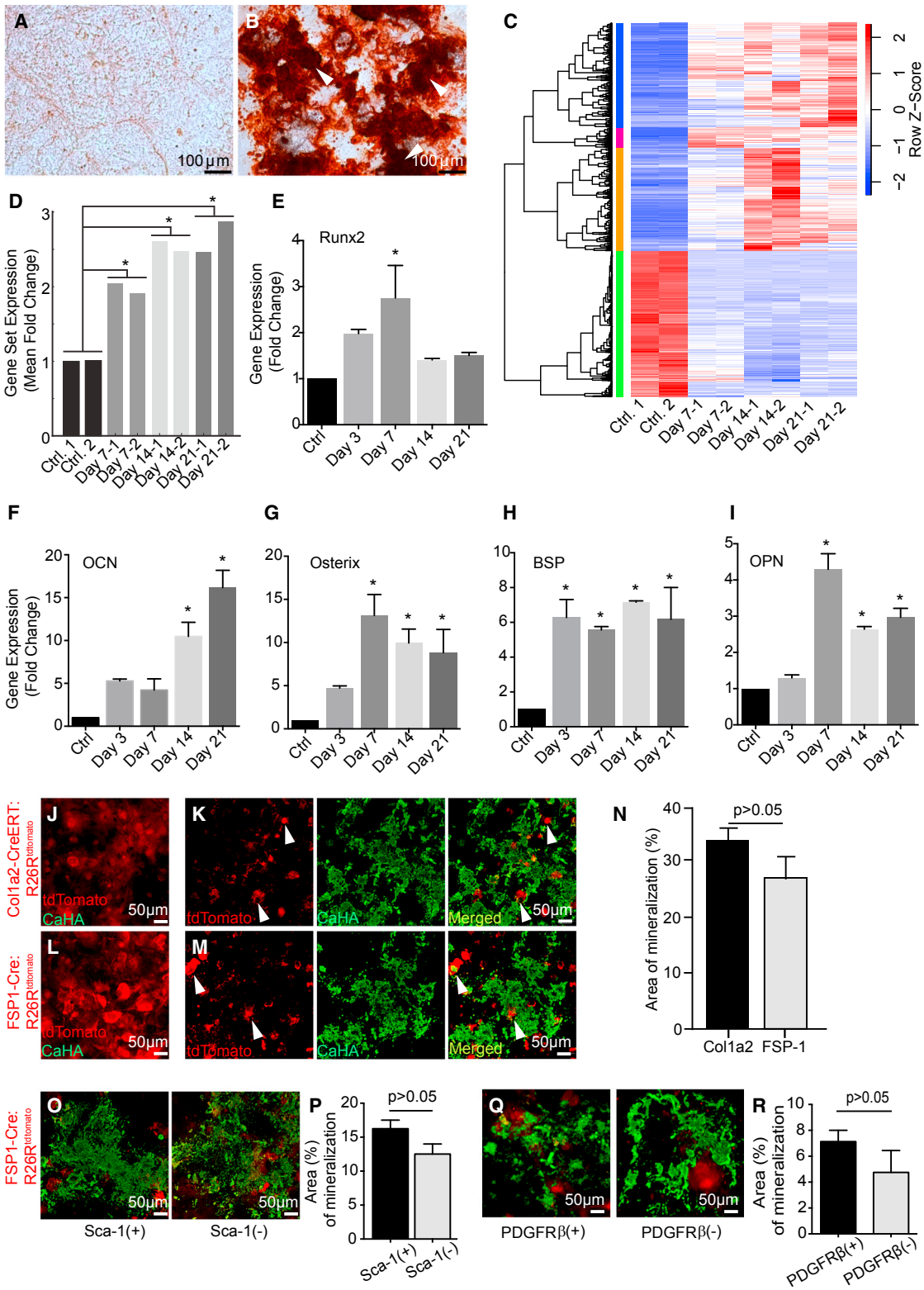

Figure 1. Cardiac Fibroblasts Can Adopt Osteogenic Cell-like Fates and Contribute to Calcification In Vitro

(A and B) Cardiac fibroblasts (CFs) stained with Alizarin Red following 21 day treatment with (A) control medium or (B) osteogenic differentiation medium (arrowheads point to calcium deposition) (n = 20).

(C) Heatmap of temporal changes in gene expression of CFs undergoing osteogenic differentiation. Each row represents the scaled expression level of a gene across the 21-day differentiation period with red designating high expression and blue designating low expression. The genes are clustered into four main

(legend continued on next page)

osteoblast cell-like fates and directly contribute to calcification of the heart muscle.

RESULTS

CFs Adopt Osteogenic Cell-like Fates and Induce Calcification In Vitro

To test this hypothesis, we subjected CFs (isolated from 8-week-old, male and female C57BL/6J murine hearts) to osteogenic differentiation. Osteogenic differentiation was induced when we treated isolated fibroblasts with culture medium known to induce osteogenic differentiation of mesenchymal stem cells (Jaiswal et al., 1997). Treatment of CFs with osteogenic differentiation medium (DM) for 21 days led to deposition of calcium hydroxyapatite, visualized with Alizarin Red staining (Figure 1B). No calcium deposition occurred in CFs treated with control growth medium for the same duration (Figure 1A). Gene expression analysis by RNA-seq of CFs harvested at different time points following induction of differentiation revealed clusters of genes whose expression was significantly altered in a temporally specific manner (Figure 1C). Genes regulating the cell cycle that were highly expressed in undifferentiated CFs were downregulated at the onset of differentiation and remained at low expression levels throughout the duration of osteogenic differentiation, consistent with the principle that induction of differentiation is associated with reduced rates of proliferation (Buttitta and Edgar, 2007) (Figure 1C, Figure S1A). In contrast, genes that were minimally expressed in CFs were induced in a specific temporal manner during the course of osteogenic differentiation (Figure 1C) and included sets of genes known to regulate inflammation, extracellular matrix proteins, and cell metabolism (Figure S1A). Next, we created an osteogenic signature based on a set of 37 genes that are induced during osteogenic differentiation (Chen et al., 2012; Choi et al., 2010; Granéli et al., 2014; Harkness et al., 2011; Hoshiba et al., 2009; Liu et al., 2013; Miguez et al., 2014; Nora et al., 2012; Olivares-Navarrete et al., 2011) (Figure S1B). We used the mean fold change in expression of this set of genes to quantitatively determine an osteogenic signature and observed that compared to control CFs, CFs subjected to osteogenic differentiation progressively adopted an osteogenic signature (Figure 1D). qPCR confirmed induction of expression of canonical osteoblast genes (Runx2, osteocalcin, osterix, bone sialoprotein, and osteopontin) in CFs following osteogenic differentiation (Figures 1E–1I). We next performed experiments with endothelial cells as a control to determine whether the ability to undergo osteogenic differentiation and induce mineralization is specific to fibroblasts. We treated human arterial endothelial cells (HAECs) (Romanoski et al., 2010) and human CFs to osteogenic DM in vitro for 21 days (Figures S2A–S2D). Similarly to murine CFs, human CFs robustly induced mineralization of the matrix (Figures S2B and S2D) but HAECs under identical conditions failed to induce mineralization of the matrix (Figures S2A and S2C), suggesting that the ability to undergo osteogenic differentiation was not autonomous of the phenotype of the cell. We next investigated whether the changes in expression of osteogenic genes in CFs were reversible. We treated CFs with osteogenic DM for 14 days and then reseeded them in the presence or absence of osteogenic DM for another 14 days (Figure S2E). Expression of the canonical master osteogenic transcription factor Runx2 did not substantially change upon removal of the cells from an osteogenic environment and their placement under regular growth conditions (Figure S2F). These observations suggest that the osteogenic phenotype adopted by CFs is stable.

To confirm our in vitro observations, we isolated CFs from transgenic mice in which CFs are genetically labeled. For this purpose we crossed transgenic mice harboring a tamoxifen-inducible Cre recombinase driven by enhancer elements of the Type 1 collagen α2 gene (Col1a2-CreERT) or a Cre recombinase driven by promoter elements of the Fibroblast specific protein 1 gene (FSP1-Cre) to the lineage reporter R26R^{tdTomato} mice to create progeny, Col1a2-CreERT:R26R^{tdTomato} or FSP1-Cre:R26R^{tdTomato} mice (Qian et al., 2012; Ubil et al., 2014; Zheng et al., 2002). We have recently shown that administration of tamoxifen for 10 days in Col1a2-CreERT:R26R^{tdTomato} mice results in specific labeling of approximately 55% of CFs (Ubil et al., 2014). We isolated tdTomato-labeled CFs from Col1a2-CreERT:R26R^{tdTomato} mice (99% purity by flow cytometry) (Figures S3A and S3B), subjected labeled CFs to osteogenic differentiation (Figures 1J and 1K), and observed calcium hydroxyapatite deposition (Figure 1K), but not in labeled CFs cultured under control conditions (Figure 1J). In the FSP1-Cre:R26R^{tdTomato} transgenic mice, the FSP-1 promoter elements drive Cre recombinase and this system has been used to track fibroblast fates (Qian et al., 2012; Song et al., 2012). Labeled CFs were isolated from FSP1-Cre:R26R^{tdTomato} mice by flow cytometry (98%

groups: blue, magenta, orange, and green. The blue cluster includes 470 genes and is dominated by low expression in the control samples and peak expression at the later time point in day 14 and 21. The magenta cluster includes 91 genes and is dominated by peak expression at day 7. The orange cluster includes 466 genes and is dominated by peak expression at day 14. The green cluster includes 660 genes and is dominated by peak expression in the control samples with low expression throughout the differentiation period. (n = 2 independent cultures/time points are shown. Ctrl 1 and 2 represent control CFs harvested at Day 0.)

(D) Bar chart of the mean expression fold change of CFs undergoing osteogenic differentiation across a set of 37 osteogenic-related genes with two samples analyzed at each time point (*$p < 0.002$, compared to controls).

(E–I) q-PCR to confirm changes in expression of canonical osteoblast genes Runx2 (E), osteocalcin (OCN) (F), osterix (Osx) (G), Bone sialoprotein (BSP) (H), and osteopontin (OPN) (I) in CFs induced to differentiate (mean ± SEM, n = 3, *$p < 0.05$ compared to control).

(J–N) CFs isolated from Col1a2-CreERT:R26R^{tdTomato} or FSP1-Cre:R26R^{tdTomato} mice were subjected to osteogenic differentiation and wells were stained for calcium hydroxyapatite (HA) (green) following 21 day treatment with (J and L) control medium or (K and M) differentiation medium (representative images, n = 6; arrows show tdTomato-labeled CFs surrounded by calcium HA). (N) Area of mineralization induced by differentiation of CFs is labeled by the Col1a2 or FSP1-Cre drivers (n = 6).

(O) Calcium HA (green) deposition following differentiation of FSP1-labeled Sca-1+ and Sca-1− fractions and (P) quantitation of the area of mineralization (representative images, mean ± SEM, n = 6).

(Q and R) Calcium HA deposition following osteogenic differentiation of FSP1-labeled PDGFRβ+ and PDGFRβ− fractions (Q) and quantitation of the area of mineralization (R) (representative images, mean ± SEM, n = 5).

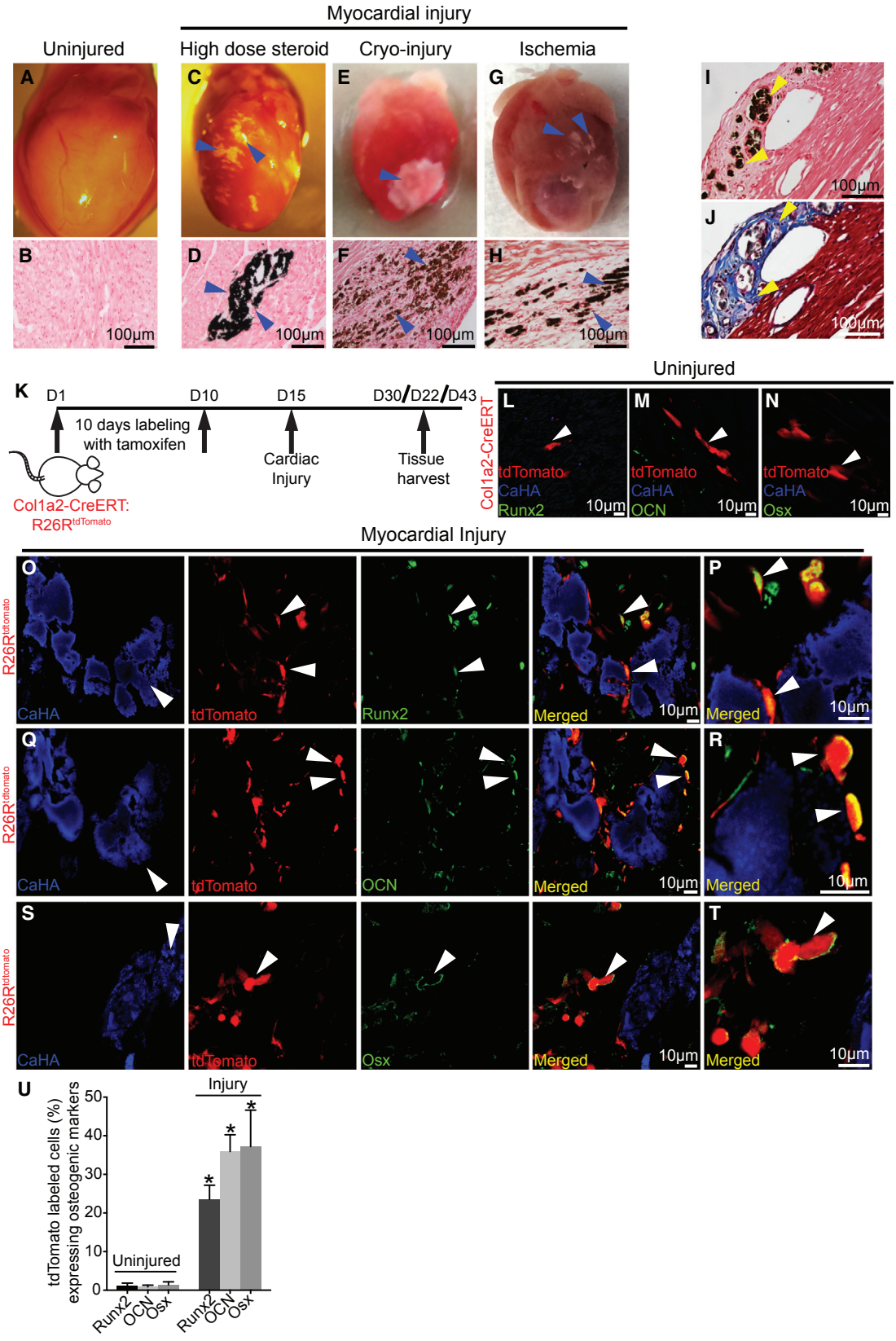

(legend on next page)

purity) (Figures S3C and S3D) and upon induction of osteogenic differentiation (Figures 1L and 1M) formed calcium hydroxyapatite (Figure 1M) while FSP1-labeled CFs under control conditions did not (Figure 1L). The extent of hydroxyapatite deposition following 21 days of osteogenic differentiation was not significantly different between FSP1-labeled and Col1a2-labeled CFs (Figure 1N), suggesting that the ability to undergo osteogenic differentiation was not dependent on the Cre drivers chosen.

We next investigated the possibility that osteogenic differentiation of genetically labeled CFs could be secondary to the presence of progenitor-like cells that undergo osteogenic differentiation. We first determined expression of the progenitor marker C-Kit in FSP1-labeled CFs but observed that 99.9% of labeled cells were negative for C-Kit expression (Figure S3E). Cardiac progenitors identified by expression of Stem cell antigen (Sca-1) are the most populous type of progenitor cell present within the mouse heart (Leri et al., 2005). More recently, a colony forming unit-fibroblast (CFU-F) has been identified in the heart to mark cardiac stromal cells with progenitor characteristics and also expresses Sca-1 (Chong et al., 2011). We isolated labeled CFs from FSP1-Cre:R26R^{tdTomato} mice and separated the tdTomato-labeled cells into predominantly Sca-1 expressing and Sca-1 negative populations (98.5% and 97% purity, respectively) by flow cytometry (Figures S3F and S3G). Consistent with CFU properties of Sca-1-expressing cells (Chong et al., 2011), we observed a significant reduction of CFU capacity of tdTomato(+)Sca-1(−) fraction compared to the tdTomato(+) Sca-1(+) fractions (Figures S3H and S3I). However, upon osteogenic differentiation, there was no significant difference in the extent of calcium hydroxyapatite deposition between tdTomato(+)Sca-1(+) and tdTomato(+)Sca-1(−) cells (Figures 1O and 1P), thereby suggesting that osteogenic differentiation of genetically labeled fibroblasts is unlikely to be secondary to the presence of Sca-1-expressing progenitor cells.

Pericytes in organs are thought to possess multipotent progenitor cell characteristics (Crisan et al., 2008), and we next determined whether pericytes potentially present in the genetically labeled fibroblast pool could have contributed to calcification. Pericytes can be identified by expression of NG2, CD146, and Platelet Derived Growth Factor Receptor β (PDGFRβ) (Murray et al., 2016). We examined sections of uninjured hearts of FSP1-Cre:R26R^{tdTomato} mice but observed minimal expression of NG2 (98.4% of tdTomato cells negative for NG2) or CD146 (99.2% of tdTomato cells negative for NG2) in tdTomato-labeled cells (Figures S4A–S4F). With flow cytometry, we did observe a fraction of FSP1-labeled cells to express PDGFRβ and separated the cells into tdTomato(+)PDGFRβ enriched and tdTomato(+)PDGFRβ depleted cells (Figures S4G and S4H). Upon osteogenic differentiation, the extent of hydroxyapatite deposition was similar in FSP1-labeled PDGFRβ enriched and FSP1-labeled PDGFRβ depleted pools (Figures 1Q and 1R), thus demonstrating that PDGFRβ-expressing cells are not the predominant source of cells in the fibroblast pool undergoing osteogenic differentiation. Taken together, these observations suggest that CFs isolated from the adult murine heart can adopt osteogenic cell-like fates and contribute to calcium deposition in vitro.

Osteogenic Differentiation of CFs in Multiple Murine Models of Myocardial Calcification

We next investigated whether CFs can adopt osteoblast cell-like fates in vivo and directly contribute to ectopic calcification of the myocardium. To address this question, we created three murine models of myocardial calcification and determined with lineage tracing techniques whether genetically labeled CFs adopted an osteoblast phenotype and contributed to heart calcification in vivo. Cardiac injury or aging in certain strains of mice (e.g., C3H/HeJ, BALB/cByJ, and DBA/2J) can lead to the development of calcification within the myocardium (Glass et al., 2013; Ivandic et al., 1996; Korff et al., 2006). We used several different methods to induce myocardial injury in the C3H strain of mice. First, we administered high-dose systemic steroids daily for 10 days, which is known to induce myocyte necrosis (Sparks et al., 1955). Uninjured hearts did not exhibit any calcification (Figures 2A and 2B), but animals injected with steroids exhibited patchy cardiac calcification within 5 days of cessation of steroid injections (Figures 2C and 2D). Cryo-probe-mediated injury of the mid ventricle (Aherrahrou et al., 2004) also resulted in calcification of the injury region within 7 days of injury (Figures 2E and 2F). Finally, ischemic injury of the myocardium by ligation of the left anterior descending (LAD) coronary artery (Korff et al., 2006) led to patchy calcification of the injury region within 4 weeks of ischemic insult (Figures 2G and 2H). Consistent with the known association of fibrosis and calcification, we observed calcification only in regions where there was fibrosis (identified by Masson's trichrome staining) (Figures 2I and 2J).

Next we induced injury in the Col1a2-CreERT:R26R^{tdTomato} transgenic mice to determine whether fibroblasts adopted an

Figure 2. CFs Can Adopt Osteogenic Cell-like Fates in Murine Models of Myocardial Calcification

(A–H) Hearts of C3H mice demonstrating absence of any calcification in the uninjured state (A and B), but calcific lesions following high-dose systemic steroids (C and D), cryo-injury (E and F), or ischemic injury (G and H) appear (blue arrowheads; representative images, n = 15). In (B), (D), (F), and (H), Von Kossa staining identifies calcium deposition.

(I and J) Region of myocardial calcification (following systemic steroids) stained with Von Kossa (I) or Masson's trichrome (J) showing region of calcification (I, arrowheads) associated with collagen deposition (J, arrowheads).

(K) Experimental strategy for labeling CFs and induction of cardiac calcification.

(L–N) Uninjured hearts of Col1a2-CreERT:R26R^{tdTomato} mice do not have calcium (blue), nor do labeled fibroblasts (arrowheads) express osteogenic markers (green).

(O–T) Expression of osteogenic markers in labeled CFs following systemic steroid administration. Regions of calcification within the heart showing calcium HA formation within the myocardium (blue, arrowheads), tdTomato-labeled cardiac fibroblasts (red, arrowheads), and cells expressing the osteogenic markers Runx2 (in O), osteocalcin (in Q), and Osterix (in S) (green, arrowheads) are shown. The merged images demonstrate labeled fibroblasts expressing osteogenic markers (arrowheads). (P), (R), and (T) shows magnified images demonstrating labeled CFs expressing osteogenic markers in close proximity to the deposited calcium HA (arrowheads, representative images, n = 5).

(U) Quantitation of the fraction of tdTomato-labeled CFs expressing osteogenic markers in hearts of uninjured or steroid-injected animals (mean ± SEM, n = 3, *p < 0.05, compared to control uninjured hearts).

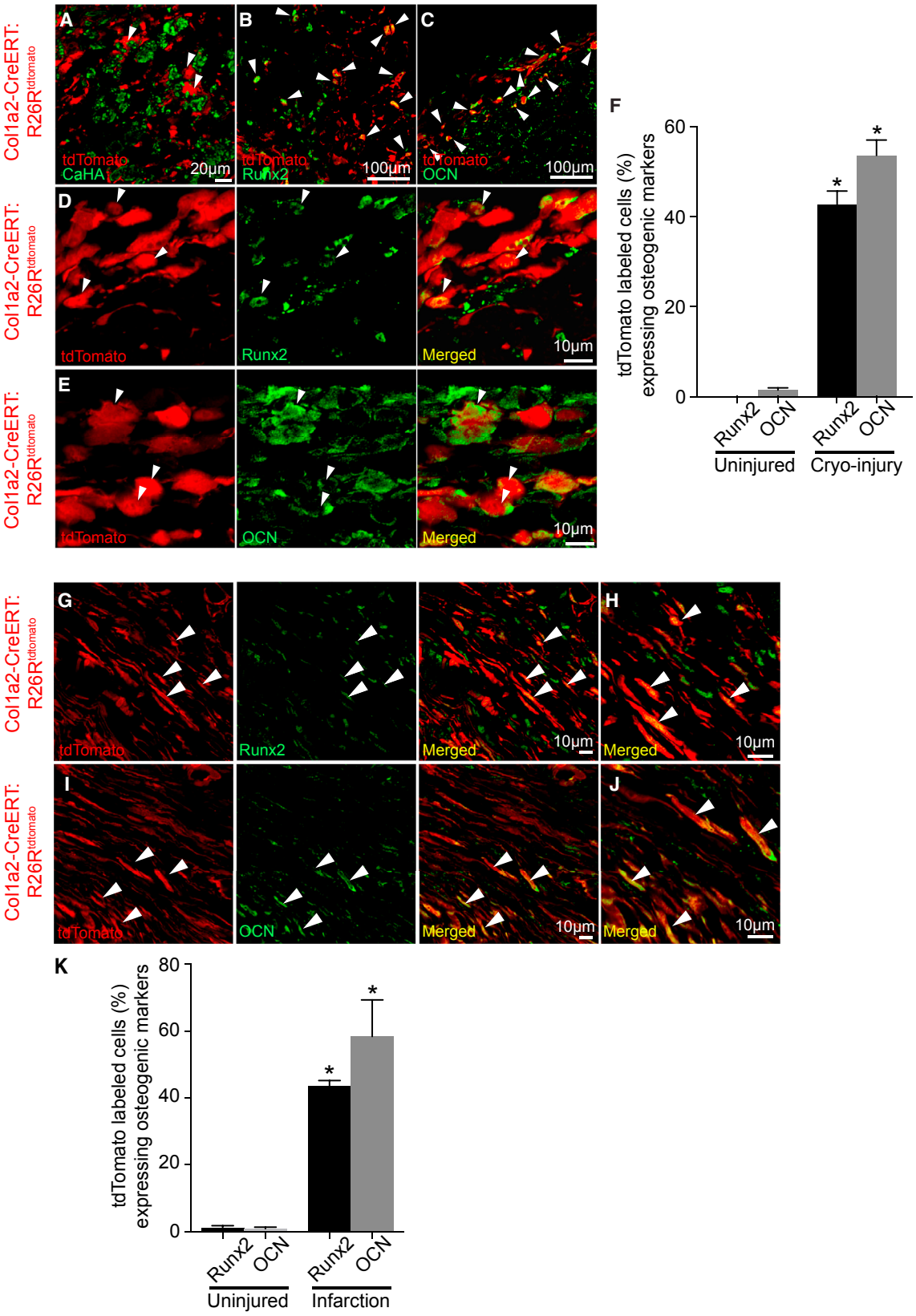

(legend on next page)

osteoblast fate and contributed to myocardial calcification. For this purpose the Col1a2-CreERT:R26R^{tdTomato} mice (B6 background) were backcrossed to a C3H background for 8–10 generations to obtain a robust calcification phenotype after heart injury. Tamoxifen was administered for 10 days to 8-week-old animals to label CFs, and following a 5 day gap, myocardial injury was induced with hydrocortisone, cryo-probe, or permanent ligation of the LAD coronary artery, and tissue was harvested at 5 days following completion of hydrocortisone injections or 7 days and 4 weeks after cryo and ischemic injury, respectively (Figure 2K). In uninjured hearts of Col1a2-CreERT:R26R^{tdTomato} mice, tdTomato-labeled CFs did not express the canonical osteogenic markers Runx2, osteocalcin (OCN), or osterix (Figures 2L–2N). In the model of cardiac calcification induced by systemic high-dose steroids, tdTomato-labeled CFs expressed the master osteogenic transcription factor Runx2 and osteoblast markers osteocalcin and osterix and were arranged in close physical apposition to calcium hydroxyapatite deposits (Figures 2O–2T). The extracellular matrix protein osteopontin has been implicated in the regulation of ectopic cardiac calcification and we observed abundant osteopontin expression in labeled fibroblasts adjacent to calcified myocardium (Figures S5A–S5E). We analyzed the expression of osteogenic markers by tdTomato-labeled CFs within the region of calcification and observed that 23.5% ± 3.6%, 35.9% ± 4.3%, and 37.9% ± 9.4% (mean ± SEM) of labeled CFs expressed the markers Runx2, OCN, and osterix, respectively, while the fraction of labeled CFs expressing these markers in uninjured hearts was less than 1.5% ($p < 0.05$) (Figure 2U). In cryo and ischemic injury-induced myocardial calcification, we similarly observed a substantial fraction of labeled CFs to express osteogenic markers. The fraction of labeled CFs expressing osteogenic markers (Runx2 and OCN) was approximately 42.7% ± 3% and 53.6% ± 3.4% for cryo injury (mean ± SEM) (Figures 3A–3F) and 43.5% ± 1.7% and 58.4% ± 10.9% for ischemic injury (mean ± SEM) (Figures 3G–3K), with expression of these markers in the control uninjured hearts at less than 1% of labeled fibroblasts ($p < 0.05$) (Figures 3F and 3K). The number of Runx2+ cells not labeled by tdTomato was approximately 38% after injury; that could reflect limitations with efficiency of Cre labeling or unlabeled fibroblasts expressing osteogenic markers.

To corroborate our findings with the Col1a2-CreERT mice, we used the TCF21-MerCreMer:R26R^{tdTomato} mouse (backcrossed to a C3H background), which has been used to specifically label CFs in the adult heart (Acharya et al., 2011; Kanisicak et al., 2016). In uninjured hearts injected with tamoxifen, tdTomato-labeled cells did not express Runx2 or OCN (Figures 4A and 4B). However, following cryo injury, we observed that substantial numbers of tdTomato-labeled CFs in the region of injury expressed osteogenic markers (Figures 4C–4E), corroborating our findings with the Col1a2-CreERT driver. As calcification occurs in the region of injury, we also performed immunostaining to determine expression of Runx2 in myocytes, but we did not observe any myocytes expressing Runx2 (Figures S5F–S5H). We also did not observe any evidence of intravascular calcification (Figures S5I–S5K). Finally, in strains of mice (B6) that do not exhibit calcification after injury, labeled CFs did not express any osteogenic markers, demonstrating that expression of osteoblast markers in CFs is not simply a response to injury but is associated with the calcific phenotype (Figures S5L and S5M). Collectively these in vivo experiments using fate mapping with independent Cre drivers and multiple models of myocardial calcification suggest that CFs can adopt an osteoblast cell-like fate.

CFs Directly Induce Mineralization of the Affected Tissue

Osteoblasts not only express extracellular matrix proteins, but also directly contribute to the mineralization of the extracellular matrix. We next investigated whether CFs in regions of myocardial calcification can directly contribute to mineralization of extracellular matrix. To address this question, we dissected regions of myocardial calcification following cryo-injury in Col1a2-CreERT:R26R^{tdTomato} mice and performed in vitro explant culture of calcified myocardial tissue (Figure 5A). We observed that tdTomato-labeled CFs migrated outward from the control or calcified myocardial tissue (Figure 5B). Immunofluorescent staining showed that 24.8% ± 2.9% and 64.7% ± 3% (mean ± SEM) of tdTomato-labeled CFs that had migrated from the calcific explant culture expressed Runx2 and OCN (Figures 5C–5E). In contrast, tdTomato-labeled CFs migrating from explanted myocardial cultures of non-injured hearts did not express osteogenic markers (Figure 5E). Labeled fibroblasts (tdTomato+) from the control or calcified myocardial explanted tissue were then sorted by flow cytometry to 99% purity and injected into subcutaneous pockets surgically fashioned on the dorsum of mice (Abdallah et al., 2008) (recipient mice were wild-type C3H strain, no tdTomato transgene present) (Figure 5F). As a control, we isolated CFs from explant cultures of uninjured heart tissue of Col1a2-CreERT:R26R^{tdTomato} mice and implanted them in an identical manner in a subcutaneous pocket

Figure 3. CFs Express Osteogenic Markers in Myocardial Calcification Induced by Cryo-Injury or Myocardial Infarction

Col1a2-CreERT:R26R^{tdTomato} mice (C3H background) were subjected to cryo-injury (A–F) or myocardial infarction (G–K) and the calcified region of the heart was analyzed.

(A) Section through the calcified injured region demonstrates abundant tdTomato cells (red, arrows) present within deposits of calcium hydroxyapatite (green).

(B and C) Low-magnification images of tdTomato-labeled CFs expressing Runx2 (B) and OCN (C) (representative images, n = 5).

(D and E) Higher-magnification images of tdTomato-labeled CFs (arrows) expressing Runx2 (D) or OCN (E) with merged image demonstrating colocalization of fluorophores (arrows).

(F) Quantitation of the fraction of labeled CFs expressing Runx2 and OCN in uninjured versus cryo-injured calcific regions (mean ± SEM, n = 3, *$p < 0.001$ compared to uninjured control hearts).

(G–K) Immunofluorescent staining of calcific regions of infarcted hearts of Col1a2-CreERT:R26R^{tdTomato} animals 4 weeks after infarction shows tdTomato-labeled cells (arrows) in area of calcification expressing (G) Runx2 with merged image showing tdTomato cells expressing Runx2 (arrows). (H) displays higher magnification of (G); (I) displays OCN with merged image demonstrating tdTomato cells expressing OCN (arrows), and (J) displays same in higher magnification. (K) shows quantitation of the fraction of tdTomato-labeled CFs expressing Runx2 or OCN in uninjured and calcified regions of infarcted hearts (mean ± SEM, n = 3, *$p < 0.01$ compared to control uninjured hearts).

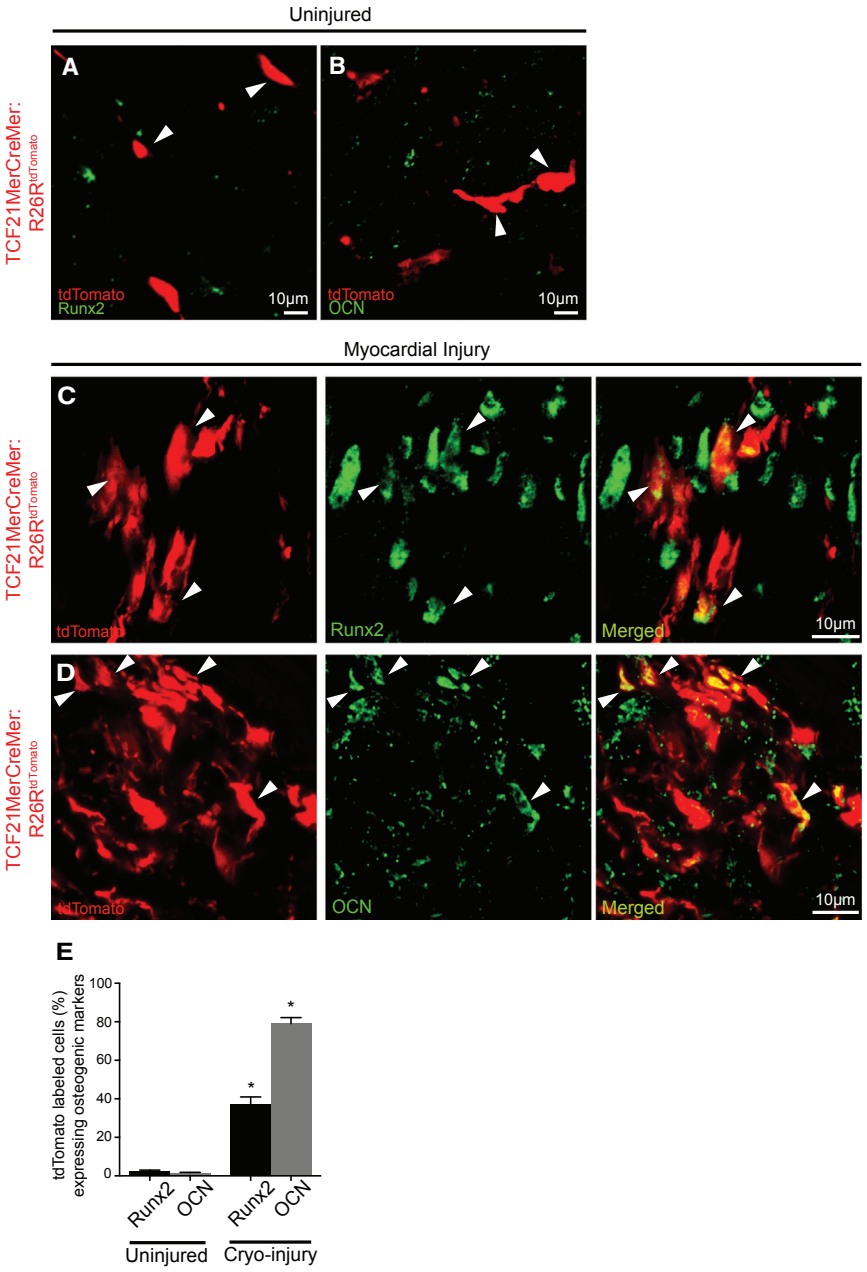

Figure 4. CFs Identified by the TCF21 Label Express Osteogenic Markers following Cryo-Injury-Induced Cardiac Calcification

(A and B) Heart sections of tamoxifen-injected but uninjured TCF21-MerCreMer:R26R^{tdTomato} (C3H background) hearts show tdTomato cells not expressing Runx2 (A) or OCN (B).

(C and D) Immunofluorescent staining of injured calcified regions shows multiple tdTomato-labeled cells expressing (C) Runx2 or (D) OCN (merged image, arrowheads) (representative images, n = 3).

(E) Quantitation of tdTomato-labeled CFs expressing Runx2 and OCN in calcified regions versus that of uninjured TCF21-MerCreMer:R26R^{tdTomato} mice (mean ± SEM, n = 3, *p < 0.05).

fashioned on the contralateral side of the same animal (Figure 5G). Finally another subcutaneous dorsal pocket was created to receive injected medium without any cells (Figures 5A and 5G). We subjected the animals to Computer Associated Tomography (micro-CT) at weekly intervals. At 4 weeks after implantation, we observed a significantly greater degree of calcification of the subcutaneous region injected with labeled CFs isolated from calcific myocardial tissue compared to subcutaneous tissue injected with labeled fibroblasts from uninjured animals or not injected with fibroblasts (Figures 5H–5J and Movie S1). There was no difference in the degree of calcification between subcutaneous pockets injected without cells or with tdTomato-labeled cells isolated from explant culture of uninjured myocardium (Figure 5J). To confirm that the increase in calcification represented new osteogenic activity, we performed positron emission tomography (micro-PET) with ^{18}NaF radionuclide, which binds to calcium hydroxyapatite in newly formed bone and is used in clinical practice to identify regions of new bone formation (Czernin et al., 2010). We observed a significant and marked increase in PET signal in subcutaneous tissues injected with labeled CFs isolated from calcified myocardial tissue compared to control groups (Figures 5K and 5L) and the anatomic location of the enhanced signal colocalized with the region of subcutaneous calcification noted on the CT scan (Figure 5L).

We next dissected the calcified subcutaneous tissue to determine the presence of tdTomato-labeled osteogenic cells. Histological stains (Von Kossa and Hematoxylin) identified subcutaneous calcific deposits (Figures 5M and 5N). On immunofluorescent staining, we observed abundant tdTomato-labeled cells expressing osteogenic markers OCN and Runx2 present on the edges of calcified matrix (Figures 5O–5T). These cell transplantation experiments demonstrate that CFs harvested from calcific, but not uninjured, myocardium, when injected into soft tissues, are sufficient to induce ectopic soft tissue calcification, showing a direct role of the CF in mediating soft tissue calcification.

A Disparate Injury Response Underlies Pathological Cardiac Calcification

Having demonstrated that CFs can induce mineralization of the matrix, we investigated mechanisms of osteogenesis or mineralization that could be potentially targeted to decrease ectopic calcification. We performed RNA-seq on uninjured and injured cardiac regions of C3H strains (calcify after injury) and B6 strains (no calcification after injury) (Figure S6A). Gene expression analysis demonstrated that calcific hearts compared to non-calcific

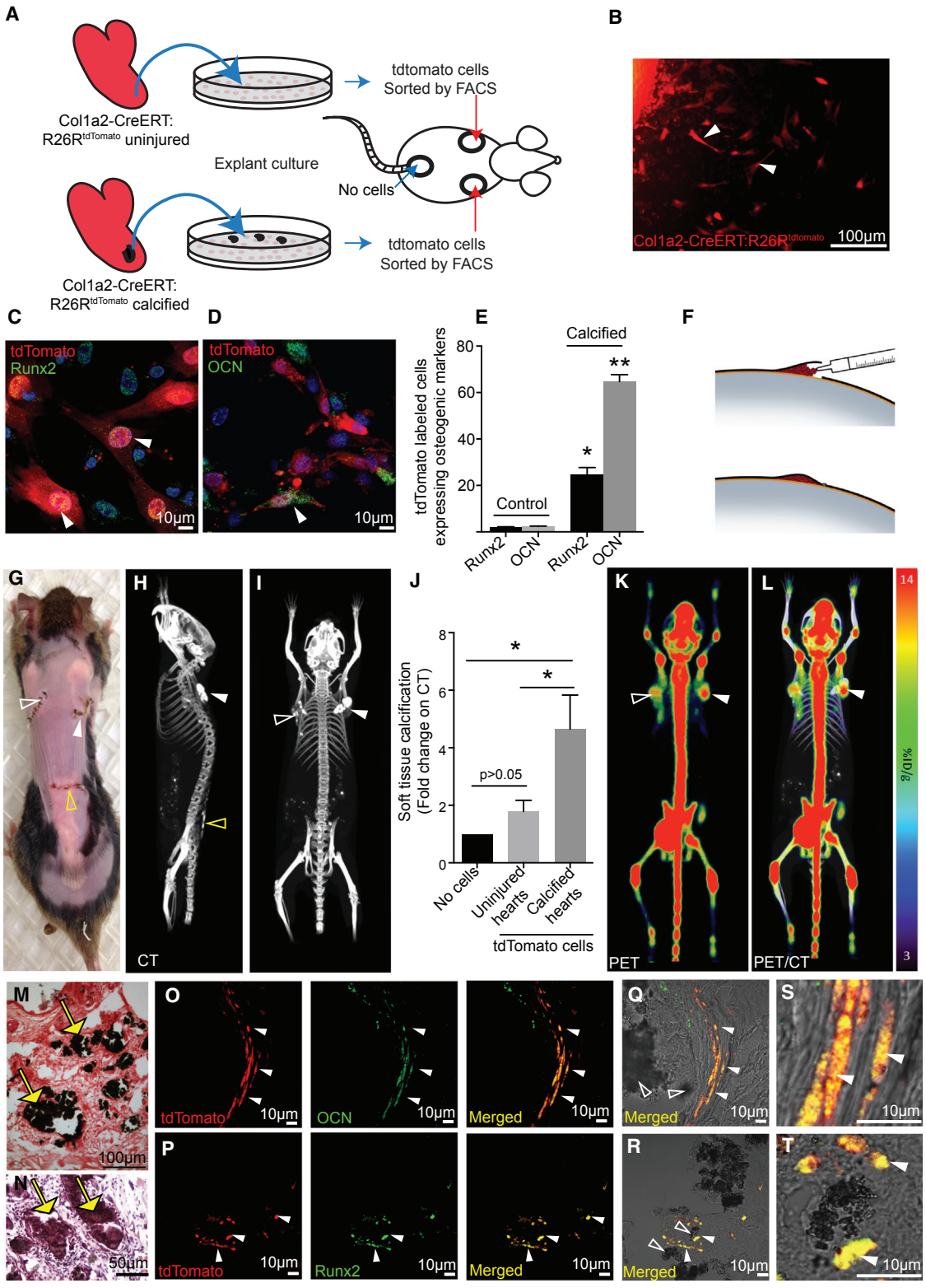

Figure 5. Fibroblasts Isolated from Calcific Heart Lesions Can Induce Soft Tissue Calcification When Injected into Another Host

(A) Experimental strategy where genetically labeled CFs harvested following explant culture of calcified or uninjured myocardium are injected into subcutaneous pockets fashioned on the dorsum of animals. Medium without cells is injected into a third pocket over the lower dorsum.

(B) Explant culture of calcified myocardial lesion (cryo-injury induced) with tdTomato-labeled CFs migrating from the lesion (arrowheads).

(C and D) Migrating tdTomato-labeled cells expressing Runx2 (C) and OCN (D) (green, arrowheads).

(legend continued on next page)

hearts responded to injury with a dramatically different transcriptional program. In contrast to only 70 odd genes that were differentially upregulated following injury in non-calcified mouse hearts (B6), about 960 genes were upregulated in C3H hearts following injury-induced calcification (Figure S6B). Out of the 960 differentially upregulated genes, only 35 were found to be common or upregulated in both C3H and B6 hearts after injury (Figure S6B), illustrating the overlapping but dramatically different magnitude of the injury response. Families of genes regulating diverse aspects of an injury response including inflammation, extracellular matrix proteins, cell proliferation, and collagen production were differentially expressed between the calcific and non-calcific hearts after injury (Figure S6C). We examined the expression of a set of osteogenic genes used by us earlier (Figure S1B) to represent an osteogenic signature (Figure S6D) and observed that the mean expression of osteogenic genes (osteogenic signature) was significantly higher in injured C3H hearts compared to uninjured C3H hearts (Figure S6E). The osteogenic signature was not higher in injured B6 hearts compared to control uninjured B6 hearts (Figure S6E). B6 mouse hearts had only 1 osteogenic gene that was upregulated (Figure S6F); in contrast, C3H hearts had 11 osteogenic genes upregulated after injury (Figure S6G). Runx2, Enpp1, Col1a1, and Fibronectin were upregulated genes that are well recognized to regulate osteogenesis in the skeleton (Figure S6G).

Inhibition of ENPP1-PPi-Pi Axis Attenuates Pathological Cardiac Calcification

Calcification of the extracellular matrix is critically regulated by the balance of extracellular phosphate (Pi) and pyrophosphate (PPi) (Terkeltaub, 2001). Pyrophosphate is generated at the cell surface by the enzyme ectonucleotide pyrophosphatase/phosphodiesterase-1 (ENPP1) that breaks down ATP to AMP and PPi. Pyrophosphate is well recognized to inhibit calcium hydroxyapatite mineralization (Rutsch et al., 2011) in non-skeletal tissues, but in bone and teeth, pyrophosphate promotes mineralization by serving as a substrate for tissue non-specific alkaline phosphatase that hydrolyzes pyrophosphate to generate inorganic phosphate (Terkeltaub, 2006). ENPP1 is expressed in osteoblasts, is thought to regulate osteoblast maturation and bone mineralization, and animals deficient in ENPP1 have decreased mineralization of long bones (Johnson et al., 2003). Considering the importance of ENPP1 in mineralization of the skeleton, we examined whether ENPP1, a gene identified by us to be differentially expressed (by RNA-seq) between calcific and non-calcified cardiac regions, was contributing to ectopic cardiac calcification. We first confirmed our observation and subjected C3H mice and B6 mice to cryo-induced cardiac injury. We observed with qPCR that injury increased ENPP1 expression in both C3H and B6 mouse hearts ($p < 0.05$, $n = 6$), but the increase in ENPP1 expression after injury was significantly higher in C3H hearts compared to B6 mice that did not exhibit cardiac calcification after injury ($p < 0.01$, $n = 6$) (Figure 6A). Immunostaining for ENPP1 confirmed that ENPP1 was expressed in uninjured B6 hearts (Figure 6B) and was more abundant following injury (Figure 6C). Compared to uninjured C3H hearts (Figure 6D), ENPP1 expression was markedly increased in injured C3H mouse hearts (Figure 6E). We next determined whether CFs in the injury region were a source of increased ENPP1 expression. We subjected Col1a2-CreERT:R26R^{tdTomato} mice hearts to cardiac injury and observed abundant expression of ENPP1 by tdTomato-labeled CFs in calcified regions (Figures 6F–6H). Extracellular pyrophosphate generated by ENPP1 can induce mineralization of tissues by precipitating out as calcium pyrophosphate dihydrate (CPPD) or serving as a substrate for phosphate generation and formation of calcium hydroxyapatite. To distinguish between these two, we performed Raman spectroscopy (Chen et al., 2009) and observed that the myocardial calcific deposits comprised calcium hydroxyapatite and not pyrophosphate dihydrate (Figure 6I). PPi generated by ENPP1 can be hydrolyzed by tissue non-specific alkaline phosphatase (TNAP) to Pi. The heart is known to express TNAP and we confirmed that both injured and uninjured cardiac tissue is rich in TNAP (Figures S7A and S7B). We measured gene expression and enzymatic activity of

(E) Quantification of the fraction of migrating tdTomato-labeled CFs expressing Runx2 or OCN (representative images, n = 3, mean ± SEM, n = 8, *$p < 0.01$ and **$p < 0.001$ compared to fibroblasts from uninjured animals).

(F) Surgical technique of injecting tdTomato-labeled cells into subcutaneous pocket, where a single incision and blunt dissection was performed to create a pocket and was sutured to close the pocket following injection of cells.

(G) Dorsum of representative animal demonstrating typical sites of injection (solid arrowhead: area of injection of tdTomato cells isolated from calcific myocardium; unfilled arrowhead: area of injection of tdTomato cells isolated from uninjured myocardium; yellow unfilled arrowhead: area of injection of medium without cells).

(H and I) CT scan showing (H) lateral view with minimal calcification noted in region of injection of medium without cells (yellow unfilled arrowhead) and robust calcification in area injected with labeled fibroblasts from calcific myocardium (solid arrowhead) and (I) antero-posterior view demonstrating minimal calcification on region injected with labeled fibroblasts from uninjured myocardial explant cultures (unfilled arrowhead) in contrast to that which received an injection of cells from calcific myocardium (solid arrowhead).

(J) Quantification of the extent of calcification expressed as a fold change compared to a region injected without cells. Fold change was calculated by comparison of the density of calcification in Hounsfield units (mean ± SEM, n = 8, *$p < 0.05$, one-way Anova with Tukey's post test analysis).

(K) ^{18}NaF PET scan demonstrating increased signal in region injected with labeled fibroblasts from calcific myocardium (solid arrowhead) compared to that injected with fibroblasts from uninjured myocardium (unfilled arrowhead) (representative images, n = 8).

(L) Merged PET/CT scan demonstrating colocalization of PET signal in region of subcutaneous soft tissue calcification seen on CT (arrowhead) (PET signals are normalized to injected dose [ID] and images are presented as percent injected dose per gram (%ID/g).

(M and N) Histological staining of subcutaneous calcific tissue dissected from dorsal subcutaneous pocket with (M) Von Kossa and (N) Hematoxylin-eosin stains identifies areas of calcification (yellow arrows).

(O–T) Immunofluorescent staining of calcific region in dissected subcutaneous tissue shows expression of (O) OCN or (P) Runx2 by tdTomato-labeled cells (arrowheads) with corresponding merged images with bright field demonstrating expression of OCN (Q) or Runx2 (R) by tdTomato-labeled cells (solid arrowheads) residing on edges of calcific deposits (unfilled arrowheads). (S) and (T) are higher magnifications of the merged images with bright field showing tdTomato-labeled cells expressing OCN (S) or Runx2 (T) (representative images, n = 4).

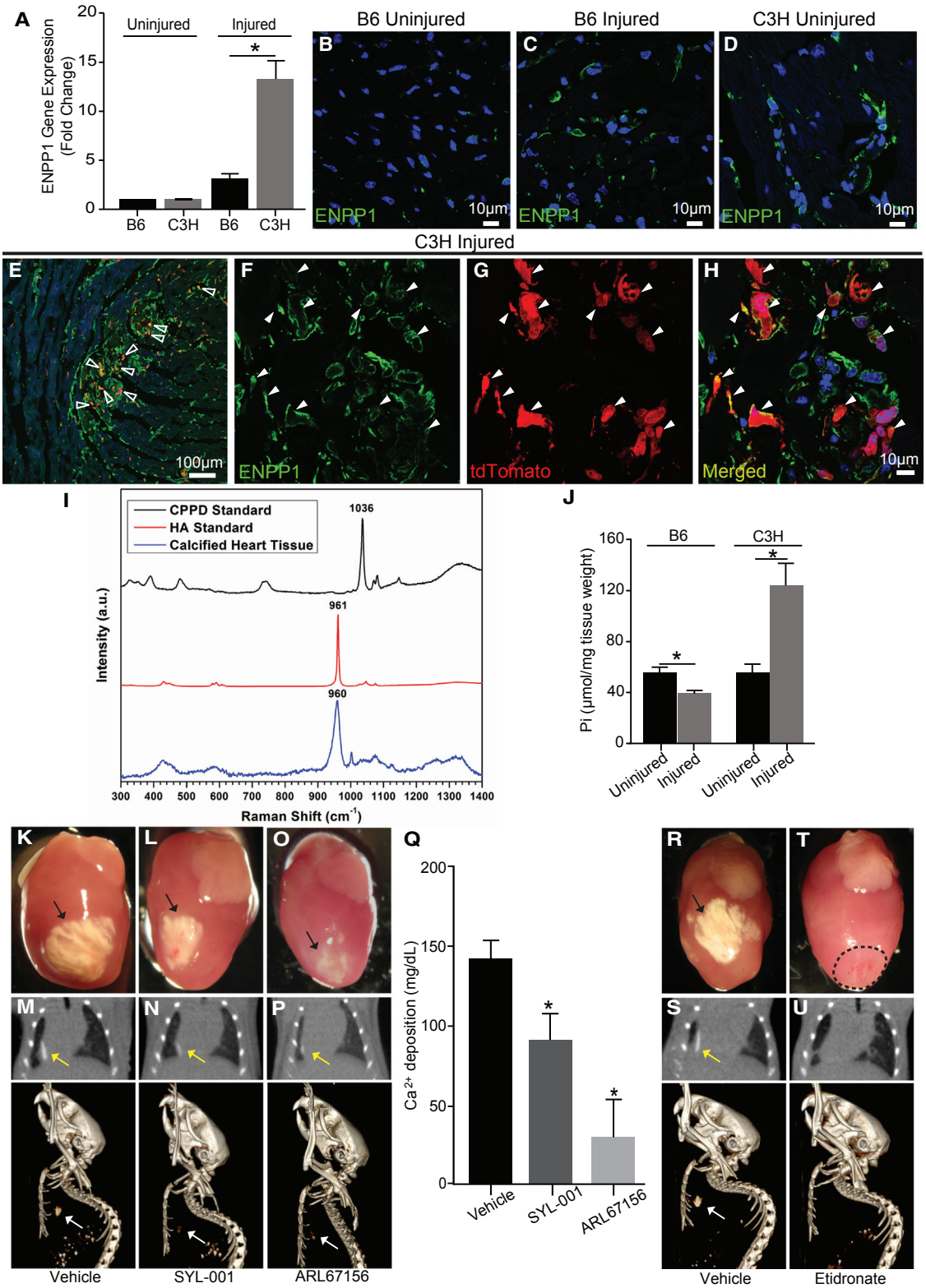

Figure 6. Role of ENPP1-PPi-Pi Axis in Ectopic Cardiac Calcification

(A) Expression of ENPP1 by qPCR in injured and uninjured regions of hearts of B6 and C3H mice 7 days after cryo-injury (mean ± SEM, n = 6, *p < 0.01).

(B–D) Immunofluorescent staining for ENPP1 in uninjured B6 heart (B), injured B6 heart (C), and uninjured C3H heart (D) (green).

(legend continued on next page)

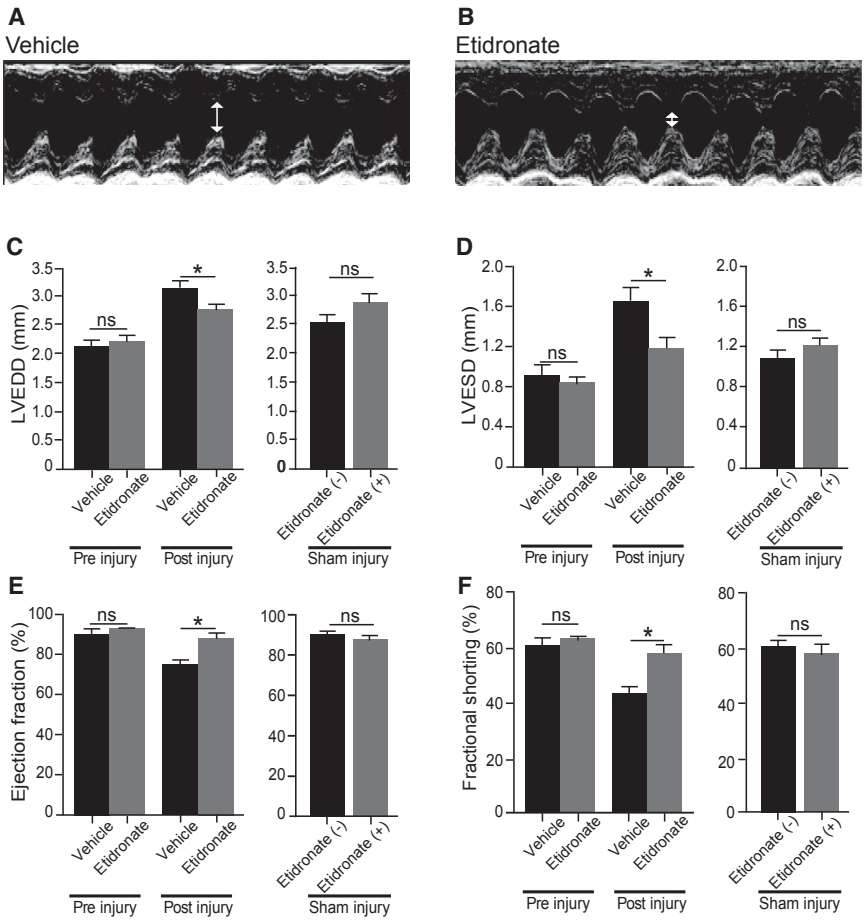

Figure 7. Inhibition of Calcification following Injury Is Associated with Better Preservation of Cardiac Function

(A and B) 2D echocardiography 7 days after cardiac cryo-injury in C3H mice treated with either (A) vehicle or (B) etidronate (representative images of n = 6 animals for vehicle and n = 8 animals for etidronate).

(C–F) Quantitation of left ventricular end diastolic dimension (LVEDD) (C) and left ventricular end systolic dimension (LVESD) (D) with ejection fraction (E) and fractional shortening (F) pre-injury, post injury, and following sham injury in vehicle-injected and etidronate-injected animals ($p < 0.05$, mean ± SEM, n = 6 in vehicle, n = 8 in etidronate, and n = 4 in sham-injured groups, ns: $p > 0.05$).

alkaline phosphatase and observed abundant expression and activity although TNAP gene expression or activity did not change following injury (Figures S7C and S7D). Biochemical measurements confirmed significantly higher phosphate levels in calcified regions (Figure 6J). Mice that did not exhibit post injury cardiac calcification, in contrast, showed a decrease in phosphate levels in the injured region (Figure 6J), although it is difficult to ascertain from our study whether this contributes to protection from calcification or is a consequence of not exhibiting calcification.

We next investigated whether the ENPP1-PPi-Pi axis could be targeted to decrease ectopic cardiac calcification. To address this question, we injected a small-molecule inhibitor of ENPP1 (SYL-001) that has been used previously to antagonize ENPP1 in the heart (Sassi et al., 2014) (Figures 6K–6N). ENPP1 inhibitor (delivered via continuous infusion) or vehicle was administered for 2 days prior to cardiac injury and for 5 days after injury. Compared to vehicle-injected control animals (Figure 6K), animals that received the ENPP1 inhibitor SYL-001 had decreased post injury cardiac calcification evident on gross inspection (Figure 6L). Micro-CT along with 3D reconstruction (Figures 6M and 6N) showed a 42% decrease in calcific deposits in animals that received the ENPP1 inhibitor (Figure 6N) compared to vehicle-treated animals (Figure 6M). To strengthen the evidence that ENPP1 contributes to calcification, we employed another small-molecule inhibitor of ENPP1 (ARL67156) (Côté et al., 2012; Lévesque et al., 2007). ARL67156 was administered in an identical manner continuously via a mini pump. ARL67156 similar, to SYL-001, significantly inhibited calcification (Figure 6O) compared to vehicle-injected controls (Figure 6K). A CT scan demonstrated an 85% decrease in calcification (Figure 6P). Biochemical measurements demonstrated a significant 35% ($p < 0.05$) and 79% ($p < 0.05$) reduction in calcium deposits in the injured hearts of mice that received

(E–G) Immunofluorescent staining of ENPP1 in injured calcified regions of Col1a2-Cre:R26R^{tdtomato} (C3H) heart (arrowheads) (E), ENPP1-expressing cells in a higher-magnification image (F), and tdTomato-expressing fibroblasts in the same field (G).

(H) Merged image demonstrating expression of ENPP1 by tdTomato cells (arrowheads).

(I) Confocal Raman microscopy demonstrating spectra of myocardial calcific deposits (blue line) compared to that of pure CPPD (black line) and hydroxyapatite (HA, red line) crystals (n = 3).

(J) Phosphate concentrations in injured and uninjured regions of non-calcified (B6) and calcified (C3H) hearts (mean ± SEM; n = 6 animals; *$p < 0.01$).

(K–P) Cryo-injured C3H animals treated with vehicle (K and M) or ENPP1 inhibitor, SYL-001 (L and N), or ARL67156 (O and P), demonstrating calcium deposition on gross inspection (K–O) and CT scan (M–P) and following 3D reconstruction (ribs removed to visualize cardiac calcification in retrosternal region) (yellow and white arrow).

(Q) Biochemical measurements of myocardial calcium deposits (n = 6 vehicle-treated, n = 9 SYL-001, and n = 5 ARL67156 animals, mean ± SEM, *$p < 0.05$ versus vehicle-injected group).

(R–U) Cryo-injured C3H animals treated with normal saline (R and S) or etidronate (T and U) demonstrating calcification on gross inspection (R and T) and CT scan (S and U) and following 3D reconstruction (yellow and white arrow). Note complete absence of any calcium deposits in the etidronate-injected animals (representative images of n = 3 for vehicle-treated animals and n = 6 for etidronate-injected animals).

the ENPP1 inhibitors SYL-001 or ARL67156, respectively (Figure 6Q).

Bisphosphonates are compounds structurally similar to pyrophosphate where two phosphate moieties are joined by a non-hydrolyzable carbon bond rather than an oxygen bond as in pyrophosphate. Although primarily used for their anti-resorptive effect on bone, first generation bisphosphonates such as etidronate can bind to calcium hydroxyapatite in sites of active bone remodeling and, as they are not hydrolyzable, prevent further bone mineralization (Drake et al., 2008). In this manner they serve as functional antagonists of the ENPP1-PPi-Pi axis and have been used to decrease ectopic vascular calcification in rodent models of kidney disease (Lomashvili et al., 2009). We investigated whether bisphosphonates could antagonize mineralization in the injured heart. We administered etidronate 1 day prior to cardiac cryo-injury and then daily until the hearts were harvested. In contrast to vehicle-injected controls (Figures 6R and 6S), etidronate completely rescued the calcific phenotype and no calcification was seen on gross inspection or on CT scans (Figures 6T and 6U). However, etidronate, when administered after the development of calcification, did not reverse or decrease the amount of deposited calcium (data not shown).

Inhibition of Cardiac Calcification Is Associated with Better Cardiac Function

We next investigated the physiologic significance of inhibiting cardiac calcification on cardiac function. In a subset of C3H animals, we performed echocardiography to determine cardiac function prior to cardiac cryo-injury and following administration of etidronate. Inhibition of calcification by etidronate was associated with significant preservation of post injury cardiac function (Figures 7A–7F). Echocardiography demonstrated better systolic function in injured animals that received etidronate (Figures 7A and 7B; Table S1). The left ventricular end diastolic diameter (LVEDD) and end systolic diameter (LVESD) were significantly decreased post injury in etidronate-injected animals compared to vehicle-treated control animals (Figures 7C and 7D). Ejection fraction (Figure 7E) and fractional shortening (Figure 7F) were substantially better following injury in animals where calcification was inhibited with etidronate. Etidronate had no effect on sham injured hearts (Figures 7C–7F). Taken together, these experiments demonstrate the potential of targeting the ENPP1-PPi-Pi axis for inhibiting ectopic cardiac calcification and augmenting cardiac function.

DISCUSSION

Cell plasticity is known to play an important physiological role during development and wound healing (Nieto et al., 2016). Mesenchymal stromal cells from different organs have been shown to be capable of inducing calcification in vitro (Ronchetti et al., 2013). Our report suggests that aberrant plasticity of CFs after injury drive them toward an osteogenic phenotype inducing mineralization of the cardiac extracellular matrix in vivo. The results described here broadly fulfill the Koch's postulates (Evans, 1976) in causally implicating the fibroblast in pathological cardiac calcification; i.e., there is (1) the presence of CFs expressing osteoblast markers in models of cardiac calcification, but not in control hearts; (2) the induction of calcific phenotype following implantation into another host; and (3) the identification of the labeled CF from calcific lesions of the host animal.

The animal models we used are clinically germane to heart calcification in humans. Human cardiac calcification is most often seen after various types of cardiac injury (ischemic, viral, and toxic), which motivated our use of different modalities of cardiac injury in mice to elicit the phenotype. Moreover, all patients after injury do not develop cardiac calcification, hence the use of different strains of mice to determine a mechanism that is differentially regulated in calcific versus non-calcific hearts.

Our data point to the role of ENPP1 that is differentially expressed in fibroblasts of hearts developing post injury calcification. Osteoblasts express ENPP1, and ENPP1-mediated generation of PPi in bone augments mineralization via hydrolysis of PPi to generate Pi and subsequent hydroxyapatite formation. Our data suggest that similar mechanisms are likely at play in regulating ectopic cardiac calcification. Administration of small molecules that inhibit ENPP1, or a bisphosphonate, led to significantly decreased ectopic cardiac calcification and preservation of post injury cardiac function. Heart calcification is a physiologically important consequence of clinical and subclinical heart injury. Our study identifies the CF and the ENPP1-PPi-Pi axis as potential cellular and pharmacological targets for treating this pathological condition.

STAR★METHODS

Detailed methods are provided in the online version of this paper and include the following:

- KEY RESOURCES TABLE
- CONTACT FOR REAGENT AND RESOURCE SHARING
- EXPERIMENTAL MODEL AND SUBJECT DETAILS
  - Animal care and use
  - Generation of mice harboring genetically labeled fibroblasts
  - Murine models of cardiac calcification
- METHOD DETAILS
  - Isolation of cardiac fibroblasts and osteogenic differentiation in vitro
  - Echocardiography
  - RNA-seq and expression analysis
  - Immunohistochemistry, confocal imaging and quantitation
  - Confocal Raman Microscopy
  - Von Kossa and Masson's trichrome staining
  - Alkaline Phosphatase activity and Phosphate assay
  - Quantitative real-time PCR
  - Flow cytometry analysis and sorting
  - Colony forming unit (CFU) assay
  - Explant culture and Ectopic Bone formation Assay of cardiac fibroblasts
  - In vivo micro PET/CT imaging
- QUANTIFICATION AND STATISTICAL ANALYSIS
- DATA AND SOFTWARE AVAILABILITY
  - Data Resources

SUPPLEMENTAL INFORMATION

Supplemental Information for this article includes seven supplemental figures, two supplemental table, and one movie and can be found with this article online at http://dx.doi.org/10.1016/j.stem.2016.10.005.

AUTHOR CONTRIBUTIONS

I.C.L.P. and S.L. performed all experiments, obtained and analyzed data, performed statistical analysis, and assisted in preparation of the manuscript. Y.L. performed animal surgeries. J.H maintained animal colonies and assisted in in vivo experiments. M.Z. and N.D. assisted in experiments. J.L. assisted in PET and CT imaging and analysis of radiographic data. M.X., O.L., and Y.-H.X. performed Raman spectroscopy and analyzed data. Y.W. assisted in experiments. L.R created the libraries and L.L. and M.P. analyzed RNA-seq data and assisted in writing the manuscript. M.R. assisted in experiments and together with A.J.L. provided crucial reagents. A.J.L. also assisted in writing the manuscript. A.D. conceptualized the project, supervised the work, and wrote the manuscript.

ACKNOWLEDGMENTS

We thank the California Nanosystems Institute, UCLA, the Broad Stem Cell Center confocal microscopy facilities, and the Jonsson Comprehensive Cancer center Flow Cytometry facilities. This work was supported by grants from the NIH (HL129178), California Institute of Regenerative Medicine (DISC1-08790), Department of Defense (PR152219), Oppenheimer Foundation, and James Eason Cardiovascular Discovery Award to A.D. and NIH grants HL28481 and HL30568 to A.J.L. The project in part also received support from NIH/NCATS UCLA CTSI (ULTR000124). We also thank Dr. Eric Olson, University of Texas Southwestern Medical Center for providing us the TCF21-MerCreMer mice and Dr. Andrew Leask, University of Western Ontario, Canada for sharing the Col1a2-CreERT mice.

Received: April 21, 2016
Revised: August 11, 2016
Accepted: October 12, 2016
Published: November 17, 2016

REFERENCES

Abdallah, B.M., Ditzel, N., and Kassem, M. (2008). Assessment of bone formation capacity using in vivo transplantation assays: procedure and tissue analysis. Methods Mol. Biol. *455*, 89–100.

Acharya, A., Baek, S.T., Banfi, S., Eskiocak, B., and Tallquist, M.D. (2011). Efficient inducible Cre-mediated recombination in Tcf21 cell lineages in the heart and kidney. Genesis *49*, 870–877.

Aherrahrou, Z., Axtner, S.B., Kaczmarek, P.M., Jurat, A., Korff, S., Doehring, L.C., Weichenhan, D., Katus, H.A., and Ivandic, B.T. (2004). A locus on chromosome 7 determines dramatic up-regulation of osteopontin in dystrophic cardiac calcification in mice. Am. J. Pathol. *164*, 1379–1387.

Buttitta, L.A., and Edgar, B.A. (2007). Mechanisms controlling cell cycle exit upon terminal differentiation. Curr. Opin. Cell Biol. *19*, 697–704.

Chen, K.H., Li, M.J., Cheng, W.T., Balic-Zunic, T., and Lin, S.Y. (2009). Identification of monoclinic calcium pyrophosphate dihydrate and hydroxyapatite in human sclera using Raman microspectroscopy. Int. J. Exp. Pathol. *90*, 74–78.

Chen, C., Uludağ, H., Wang, Z., and Jiang, H. (2012). Noggin suppression decreases BMP-2-induced osteogenesis of human bone marrow-derived mesenchymal stem cells in vitro. J. Cell. Biochem. *113*, 3672–3680.

Choi, Y.A., Lim, J., Kim, K.M., Acharya, B., Cho, J.Y., Bae, Y.C., Shin, H.I., Kim, S.Y., and Park, E.K. (2010). Secretome analysis of human BMSCs and identification of SMOC1 as an important ECM protein in osteoblast differentiation. J. Proteome Res. *9*, 2946–2956.

Chong, J.J., Chandrakanthan, V., Xaymardan, M., Asli, N.S., Li, J., Ahmed, I., Heffernan, C., Menon, M.K., Scarlett, C.J., Rashidianfar, A., et al. (2011). Adult cardiac-resident MSC-like stem cells with a proepicardial origin. Cell Stem Cell *9*, 527–540.

Côté, N., El Husseini, D., Pépin, A., Bouvet, C., Gilbert, L.A., Audet, A., Fournier, D., Pibarot, P., Moreau, P., and Mathieu, P. (2012). Inhibition of ectonucleotidase with ARL67156 prevents the development of calcific aortic valve disease in warfarin-treated rats. Eur. J. Pharmacol. *689*, 139–146.

Crisan, M., Yap, S., Casteilla, L., Chen, C.W., Corselli, M., Park, T.S., Andriolo, G., Sun, B., Zheng, B., Zhang, L., et al. (2008). A perivascular origin for mesenchymal stem cells in multiple human organs. Cell Stem Cell *3*, 301–313.

Czernin, J., Satyamurthy, N., and Schiepers, C. (2010). Molecular mechanisms of bone 18F-NaF deposition. J. Nucl. Med. *51*, 1826–1829.

Demer, L.L., and Tintut, Y. (2014). Inflammatory, metabolic, and genetic mechanisms of vascular calcification. Arterioscler. Thromb. Vasc. Biol. *34*, 715–723.

Drake, M.T., Clarke, B.L., and Khosla, S. (2008). Bisphosphonates: mechanism of action and role in clinical practice. Mayo Clin. Proc. *83*, 1032–1045.

Evans, A.S. (1976). Causation and disease: the Henle-Koch postulates revisited. Yale J. Biol. Med. *49*, 175–195.

Glass, A.M., Coombs, W., and Taffet, S.M. (2013). Spontaneous cardiac calcinosis in BALB/cByJ mice. Comp. Med. *63*, 29–37.

Granéli, C., Thorfve, A., Ruetschi, U., Brisby, H., Thomsen, P., Lindahl, A., and Karlsson, C. (2014). Novel markers of osteogenic and adipogenic differentiation of human bone marrow stromal cells identified using a quantitative proteomics approach. Stem Cell Res. (Amst.) *12*, 153–165.

Harkness, L., Mahmood, A., Ditzel, N., Abdallah, B.M., Nygaard, J.V., and Kassem, M. (2011). Selective isolation and differentiation of a stromal population of human embryonic stem cells with osteogenic potential. Bone *48*, 231–241.

Hoshiba, T., Kawazoe, N., Tateishi, T., and Chen, G. (2009). Development of stepwise osteogenesis-mimicking matrices for the regulation of mesenchymal stem cell functions. J. Biol. Chem. *284*, 31164–31173.

Ivandic, B.T., Qiao, J.H., Machleder, D., Liao, F., Drake, T.A., and Lusis, A.J. (1996). A locus on chromosome 7 determines myocardial cell necrosis and calcification (dystrophic cardiac calcinosis) in mice. Proc. Natl. Acad. Sci. USA *93*, 5483–5488.

Jaiswal, N., Haynesworth, S.E., Caplan, A.I., and Bruder, S.P. (1997). Osteogenic differentiation of purified, culture-expanded human mesenchymal stem cells in vitro. J. Cell. Biochem. *64*, 295–312.

Johnson, K., Goding, J., Van Etten, D., Sali, A., Hu, S.I., Farley, D., Krug, H., Hessle, L., Millán, J.L., and Terkeltaub, R. (2003). Linked deficiencies in extracellular PP(i) and osteopontin mediate pathologic calcification associated with defective PC-1 and ANK expression. J. Bone Miner. Res. *18*, 994–1004.

Kanisicak, O., Khalil, H., Ivey, M.J., Karch, J., Maliken, B.D., Correll, R.N., Brody, M.J., J Lin, S.C., Aronow, B.J., Tallquist, M.D., and Molkentin, J.D. (2016). Genetic lineage tracing defines myofibroblast origin and function in the injured heart. Nat. Commun. *7*, 12260.

Korff, S., Riechert, N., Schoensiegel, F., Weichenhan, D., Autschbach, F., Katus, H.A., and Ivandic, B.T. (2006). Calcification of myocardial necrosis is common in mice. Virchows Arch. *448*, 630–638.

Langenbach, F., Berr, K., Naujoks, C., Hassel, A., Hentschel, M., Depprich, R., Kubler, N.R., Meyer, U., Wiesmann, H.P., Kögler, G., and Handschel, J. (2011). Generation and differentiation of microtissues from multipotent precursor cells for use in tissue engineering. Nat. Protoc. *6*, 1726–1735.

Leri, A., Kajstura, J., and Anversa, P. (2005). Cardiac stem cells and mechanisms of myocardial regeneration. Physiol. Rev. *85*, 1373–1416.

Lev, M. (1964). Anatomic Basis for Atrioventricular Block. Am. J. Med. *37*, 742–748.

Lévesque, S.A., Lavoie, E.G., Lecka, J., Bigonnesse, F., and Sévigny, J. (2007). Specificity of the ecto-ATPase inhibitor ARL 67156 on human and mouse ectonucleotidases. Br. J. Pharmacol. *152*, 141–150.

Liu, C., Gu, S., Sun, C., Ye, W., Song, Z., Zhang, Y., and Chen, Y. (2013). FGF signaling sustains the odontogenic fate of dental mesenchyme by suppressing β-catenin signaling. Development *140*, 4375–4385.

Lomashvili, K.A., Monier-Faugere, M.C., Wang, X., Malluche, H.H., and O'Neill, W.C. (2009). Effect of bisphosphonates on vascular calcification and bone metabolism in experimental renal failure. Kidney Int. *75*, 617–625.

Miguez, P.A., Terajima, M., Nagaoka, H., Ferreira, J.A., Braswell, K., Ko, C.C., and Yamauchi, M. (2014). Recombinant biglycan promotes bone morphogenetic protein-induced osteogenesis. J. Dent. Res. *93*, 406–411.

Murray, I.R., Baily, J.E., Chen, W.C., Dar, A., Gonzalez, Z.N., Jensen, A.R., Petrigliano, F.A., Deb, A., and Henderson, N.C. (2016). Skeletal and cardiac muscle pericytes: Functions and therapeutic potential. Pharmacol. Ther., in press. Published online September 2, 2016. http://dx.doi.org/10.1016/j.pharmthera.2016.09.005.

Nieto, M.A., Huang, R.Y., Jackson, R.A., and Thiery, J.P. (2016). Emt: 2016. Cell *166*, 21–45.

Nora, C.C., Camassola, M., Bellagamba, B., Ikuta, N., Christoff, A.P., Meirelles, Lda.S., Ayres, R., Margis, R., and Nardi, N.B. (2012). Molecular analysis of the differentiation potential of murine mesenchymal stem cells from tissues of endodermal or mesodermal origin. Stem Cells Dev. *21*, 1761–1768.

Olivares-Navarrete, R., Hyzy, S.L., Park, J.H., Dunn, G.R., Haithcock, D.A., Wasilewski, C.E., Boyan, B.D., and Schwartz, Z. (2011). Mediation of osteogenic differentiation of human mesenchymal stem cells on titanium surfaces by a Wnt-integrin feedback loop. Biomaterials *32*, 6399–6411.

Pugashetti, R., Shinkai, K., Ruben, B.S., Grossman, M.E., Maldonado, J., and Fox, L.P. (2011). Calcium may preferentially deposit in areas of elastic tissue damage. J. Am. Acad. Dermatol. *64*, 296–301.

Qian, L., Huang, Y., Spencer, C.I., Foley, A., Vedantham, V., Liu, L., Conway, S.J., Fu, J.D., and Srivastava, D. (2012). In vivo reprogramming of murine cardiac fibroblasts into induced cardiomyocytes. Nature *485*, 593–598.

Romanoski, C.E., Lee, S., Kim, M.J., Ingram-Drake, L., Plaisier, C.L., Yordanova, R., Tilford, C., Guan, B., He, A., Gargalovic, P.S., et al. (2010). Systems genetics analysis of gene-by-environment interactions in human cells. Am. J. Hum. Genet. *86*, 399–410.

Ronchetti, I., Boraldi, F., Annovi, G., Cianciulli, P., and Quaglino, D. (2013). Fibroblast involvement in soft connective tissue calcification. Front. Genet. *4*, 22.

Rostand, S.G., Sanders, C., Kirk, K.A., Rutsky, E.A., and Fraser, R.G. (1988). Myocardial calcification and cardiac dysfunction in chronic renal failure. Am. J. Med. *85*, 651–657.

Rutsch, F., Nitschke, Y., and Terkeltaub, R. (2011). Genetics in arterial calcification: pieces of a puzzle and cogs in a wheel. Circ. Res. *109*, 578–592.

Sassi, Y., Ahles, A., Truong, D.J., Baqi, Y., Lee, S.Y., Husse, B., Hulot, J.S., Foinquinos, A., Thum, T., Müller, C.E., et al. (2014). Cardiac myocyte-secreted cAMP exerts paracrine action via adenosine receptor activation. J. Clin. Invest. *124*, 5385–5397.

Shackley, B.S., Nguyen, T.P., Shivkumar, K., Finn, P.J., and Fishbein, M.C. (2011). Idiopathic massive myocardial calcification: a case report and review of the literature. Cardiovasc. Pathol. *20*, e79–e83.

Simchen, M.J., Toi, A., Silver, M., Smith, C.R., Hornberger, L.K., Taylor, G., and Chitayat, D. (2006). Fetal cardiac calcifications: report of four prenatally diagnosed cases and review of the literature. Ultrasound Obstet. Gynecol. *27*, 325–330.

Song, K., Nam, Y.J., Luo, X., Qi, X., Tan, W., Huang, G.N., Acharya, A., Smith, C.L., Tallquist, M.D., Neilson, E.G., et al. (2012). Heart repair by reprogramming non-myocytes with cardiac transcription factors. Nature *485*, 599–604.

Sparks, L.L., Rosenau, W., Macalpin, R.N., Daane, T.A., and Li, C.H. (1955). Production of dystrophic calcification of cardiac muscle in mice by hydrocortisone. Nature *176*, 503–504.

Stallion, A., Rafferty, J.F., Warner, B.W., Ziegler, M.M., and Ryckman, F.C. (1994). Myocardial calcification: a predictor of poor outcome for myocarditis treated with extracorporeal life support. J. Pediatr. Surg. *29*, 492–494.

Terkeltaub, R.A. (2001). Inorganic pyrophosphate generation and disposition in pathophysiology. Am. J. Physiol. Cell Physiol. *281*, C1–C11.

Terkeltaub, R. (2006). Physiologic and pathologic functions of the NPP nucleotide pyrophosphatase/phosphodiesterase family focusing on NPP1 in calcification. Purinergic Signal. *2*, 371–377.

Ubil, E., Duan, J., Pillai, I.C., Rosa-Garrido, M., Wu, Y., Bargiacchi, F., Lu, Y., Stanbouly, S., Huang, J., Rojas, M., et al. (2014). Mesenchymal-endothelial transition contributes to cardiac neovascularization. Nature *514*, 585–590.

Zheng, B., Zhang, Z., Black, C.M., de Crombrugghe, B., and Denton, C.P. (2002). Ligand-dependent genetic recombination in fibroblasts : a potentially powerful technique for investigating gene function in fibrosis. Am. J. Pathol. *160*, 1609–1617.

STAR★METHODS

KEY RESOURCES TABLE

REAGENT or RESOURCE	SOURCE	IDENTIFIER
Antibodies		
Runx2	Novus biologicals	NBP1-77461; RRID: AB_11003000
Osteocalcin	Abcam	ab 93876; RRID: AB_10675660
Osterix	Santacruz	sc 22536-R; RRID: AB_831618
CD146	Abcam	ab75769; RRID: AB_2143375
NG2	EMD Millipore	AB5320; RRID: AB_91789
ENPP1	Abcam	ab40003; RRID: AB_2099641
ALP	R&D Systems	AF2910; RRID: AB_664062
Osteopontin	Abcam	ab8448; RRID: AB_306566
Troponin	Santacruz	sc-8121; RRID: AB_2287642
CD31	Abcam	ab7388; RRID: AB_305905
Sca1	eBioscience	17-5981; RRID: AB_469487
PDGFRβ	eBioscience	17-1402; RRID: AB_1548743
c-Kit	BD Bioscience	561074; RRID: AB_10563203
Chemicals, Peptides, and Recombinant Proteins		
Tamoxifen	Sigma	T5648
Hydrocortisone	Sigma	H3035
SYL-001	Sigma	R4033
ARL67156	Tocris	1021868-83-6
Etidronate disodium hydrate	Sigma	P5248
Hydroxyapatite	Sigma	574791
CPPD Crystals	InvivoGen	tlrl-cppd
Von Kossa staining reagent	Abcam	ab150687
Trichrome Stain (Masson)	Sigma	HT15-1KT
Dexamethasone	Sigma	D4902
β-glycerol phosphate	Sigma	G9422
L-ascorbic acid	Sigma	A4403
Hydroxyapatite and β-tri-calcium phosphate	Berkeley Advanced Biomaterials	Bio-02G
Critical Commercial Assays		
Osmotic pump	Alzet	1007D
QuantiChrom Calcium Assay Kit	BioAssay Systems	DICA-500
OsteoImage Bone Mineralization Assay	Lonza	PA 1503
SensoLyte® pNPP Alkaline Phosphatase Assay Kit	Anaspec	AS-72146
PiPer Phosphate Assay Kit	Invitrogen	MP22061
RNeasy Plus Mini Kit	QIAGEN	74134
Reverse Transcription System	Promega	A3500
SensiMix SYBR and Fluorescein Kit	Quantace	QT615
Deposited Data		
Raw data files for RNA sequencing: Cardiac fibroblast	NCBI Gene Expression Omnibus	GEO: GSE87836
Raw data files for RNA sequencing: Heart tissue	NCBI Gene Expression Omnibus	GEO: GSE87837
Experimental Models: Cell Lines		
Mouse: primary cardiac fibroblast	This paper	N/A
Human: primary cardiac fibroblast	This paper	N/A
Human: endothelial cell	Romanoski et al., 2010	N/A

(*Continued on next page*)

Continued

REAGENT or RESOURCE	SOURCE	IDENTIFIER
Experimental Models: Organisms/Strains		
Mouse: C3H	The Jackson Laboratory	000659
Mouse: B6	The Jackson Laboratory	000664
Mouse: Col1a2-CreERT:R26RtdTomato	Ubil et al., 2014	N/A
Mouse: FSP1-Cre:R26RtdTomato	Ubil et al., 2014	N/A
Mouse: TCF21-MerCreMer	Acharya et al., 2011	N/A
Recombinant DNA		
Quantitative real-time PCR Primers	Table S2	IDT
Software and Algorithms		
DEseq	Bioconductor	1.24.0
ImageJ	NIH	1.6.0_24
WiRE 4	Renishaw	4.0
AMIDE	http://amide.sourceforge.net/	1.0.5
OsiriX version 3.8 imaging software	Pixmeo SARL	3.8
GraphPad Prism 6	GraphPad	6

CONTACT FOR REAGENT AND RESOURCE SHARING

Further information and requests for reagents may be directed to, and will be fulfilled by, the Lead Contact, Arjun Deb (adeb@mednet.ucla.edu).

EXPERIMENTAL MODEL AND SUBJECT DETAILS

Animal care and use

All animal studies were approved by the Animal Research Committee, University of California, Los Angeles. All animals were maintained at the UCLA vivarium according to the policies instituted by the American Association for Accreditation of Laboratory Animal Care. Sample size was estimated based on published reports on murine models of cardiac calcification (Aherrahrou et al., 2004). No animal was subjected to more than one procedure.

Generation of mice harboring genetically labeled fibroblasts

Three different Cre transgenic mice (Col1a2-CreERT:R26R^{tdTomato}, FSP1-Cre:R26R^{tdTomato} and TCF21-MerCreMer:R26R^{tdTomato}) were used for genetic fate mapping of cardiac fibroblasts in this study. The reporter lines were obtained by crossing Col1a2-CreERT, FSP1-Cre and TCF21-MerCreMer mice with the lineage reporter R26R^{tdTomato} mice. The Col1a2-CreERT:R26R^{tdTomato} and TCF21-MerCreMer:R26R^{tdTomato} mice (B6 background) were backcrossed with the C3H strain for 8-10 generations prior to cardiac injury for obtaining a calcific phenotype. Tamoxifen (1 mg) (Sigma,T5648) was injected intraperitoneally for 10 days in 8-10 weeks old Col1a2-CreERT:R26R^{tdTomato} and TCF21-MerCreMer:R26R^{tdTomato} to induce Cre-mediated recombination. Five days following cessation of tamoxifen, animals were subjected to cardiac injury. Littermates were used as controls. In all experiments, adult mice (both male and female), 8-10 weeks old were used. The TCF21-MerCreMer and the Col1a2-CreERT mice were used for in vivo experiments as the Cre is inducible and thus more rigorous for fate mapping. The FSP1Cre is not an inducible Cre and has been shown to label immune cells in vivo after injury and thus was not preferred for in vivo mapping.

Murine models of cardiac calcification

Three different murine models of cardiac calcification were created for this study by inducing cardiac injury by rapid freeze thaw of cardiac tissue (cryo-injury), ligation of the left anterior descending artery (myocardial infarction) or by systemic injection of high dose corticosteroids. For cryo-injury, mice were deeply anesthetized with 2% isoflurane, maintained at 1.5%–2% isoflurane, and intubated using a volume-cycled ventilator. A left thoracotomy was performed at the level of 2nd intercostal space and the exposed beating heart was frozen for 10 s by gently pressing a pre-cooled steel rod of 1mm diameter in dry ice (Aherrahrou et al., 2004; Korff et al., 2006). Freezing of cardiac tissue was confirmed by the rapid discoloration of the tissue. Seven days after injury, the hearts were harvested and processed for histological analysis.

Myocardial infarction was performed by ligating the left anterior descending (LAD) coronary artery (Ubil et al., 2014). After 28 days, the hearts were harvested and processed for histological analysis.

For corticosteroid induced cardiac injury and calcification (Sparks et al., 1955), we injected a saline suspension of 2.5 mg hydrocortisone (Sigma, H3035) daily subcutaneously for 10 days and hearts were harvested for histological analysis within 5 days of completion of steroid injections.

To determine effects of ENPP1 inhibition on ectopic cardiac calcification, a cryo injury was used. The ENPP1 inhibitor SYL-001 (Sigma, R4033) mixed in 10% propylene glycol (Sigma, W294004), was infused continuously (10mg/kg/day) via osmotic pump (Alzet, 1007D). Another ENPP1 inhibitor, ARL67156 trisodium salt, (Tocris, 1021868-83-6) was administered in an identical manner via osmotic pump at a dose of 1mg/kg/day. Control animals only received propylene glycol. Prior to cryo-injury, mice were injected with the drug for 24 hr. Following 7 days of etidronate or vehicle infusion, animals were subjected to micro CT scans to obtain quantitative estimates of calcium deposition. Animals were subsequently sacrificed, hearts harvested to determine calcium deposition by gross inspection and biochemical assays. For estimation of calcium deposits, calcified tissue was dried overnight and homogenized in 0.6mM HCL. After 24 hr incubation, calcium ion in supernatants was quantified by QuantiChrom Calcium Assay Kit (BioAssay Systems, DICA-500).

To determine effects of bisphosphonate, Etidronate disodium hydrate (Sigma, P5248) was administrated intraperitoneally to 9-11 weeks old C3H mice at a dose of 80mg/kg/day for 2 days and then at 30mg/kg/day till animals were harvested. On the second day of etidronate administration, mice were subjected to cryo injury of the heart. Animals were subjected to CT scanning 5 days later and subsequently hearts were harvested to determine extent of calcification.

For the generation of murine models of cardiac calcification, both male and female mice aged between 8-12 weeks were used. Control groups of mice were obtained from the same litter and the mice randomly allocated either to control or experimental arm.

METHOD DETAILS

Isolation of cardiac fibroblasts and osteogenic differentiation in vitro

Cardiac fibroblasts were isolated as described previously (Ubil et al., 2014). Briefly, hearts from euthanized uninjured mice were washed 3 times with ice cold 1X HBSS (GIBCO). Fibroblasts were isolated from human heart tissue that is perioperatively routinely discarded during ventricular assist device placement or transplantation. Heart tissue was chopped into 1mm^2 pieces and digested using 5ml of 0.1% Trypsin (GIBCO) solution with 50units/ml collagenase II (Worthington, NC9693955) at 37°C for 10 min. Five sequential digestions were performed and cells collected from 2 to 5 digestions were pooled and strained using a 40μm filter and plated in IMDM, 1X penicillin/streptomycin, 20% FBS for 2 hr at 37°C. Then medium was changed to F12K with 1X penicillin/streptomycin, 20% FBS (GIBCO), and 10ng/ml basic fibroblast growth factor (bFGF) (Millipore). Cells were maintained under these conditions until they became confluent and used for further experiments.

For osteogenic differentiation, freshly isolated cardiac fibroblasts (Passage 0 or passage 1) were plated at a density of 2.5 × 10^4 cells/cm^2 in growth medium. After overnight incubation, osteogenesis was induced using differentiation medium (α-MEM supplemented with 10% FBS, 10 nM dexamethasone (Sigma, D4902), 20 mM β-glycerol phosphate (Sigma, G9422), and 50 μM L-ascorbic acid (Sigma, A4403) (Jaiswal et al., 1997). Differentiation was visualized after 21 days either by staining with alizarin red (Sigma, A5533) or using OsteoImage (PA 1503, Lonza, Walkersville, MD, USA) (Langenbach et al., 2011) The cells were fixed in 4% paraformaldehyde and washed once with 1X PBS. The cells were again stained with 1:100 diluted OsteoImage staining solutions for 30 min at room temperature. After incubation, the cells were washed thrice with 1X wash buffer and the images were taken in a confocal laser scanning microscope (LSM 780, Zeiss). Human endothelial cells (Romanoski et al., 2010) grown in MCDB131 complete growth medium (VEC Technologies, MCDB-131C) were subjected to osteogenic differentiation under identical conditions.

For determining the area of mineralization in vitro, labeled cardiac fibroblasts were seeded onto 6cm dishes and subjected to osteogenic differentiation for 21 days. The wells were then stained with a fluorescent dye, OsteoImage (Langenbach et al., 2011) that binds to calcium hydroxyapatite and the area of fluorescence quantitated with ImageJ and expressed as a ratio to the surface area of the well. Ten random microscopic fields were examined to obtain mean area of mineralization.

Echocardiography

Echocardiography was performed on conscious animals without anesthesia. The mouse is briefly restrained manually, hair is removed from the chest and distress minimized by performing the echocardiogram rapidly. Echocardiographic imaging was done with a VisualSonics Vevo 2100 machine. Prior to conscious echocardiography, animals are acclimatized to the restraining procedure and environment by holding them in that position for about 1 min, 3 days prior to the procedure and repeating 2 days prior to the procedure.

RNA-seq and expression analysis

RNA-seq was performed on cardiac fibroblasts or cardiac tissue using standard Illumina RNA-seq library construction protocols. RNA-seq libraries were sequenced on Illumina HiSeq 2000 or Illumina Hiseq 4000. Reads were aligned to the mm9 reference genome using TopHat and gene counts were quantified with HTSeq. DESeq was used to identify differentially expressed genes of cardiac fibroblasts undergoing differentiation treatment. 1685 genes with a FDR < 0.05 and a minimum 2 fold ($\log_2$) change were subsequently clustered and visualized. A set of osteogenic genes known to be induced during bone formation or osteogenic differentiation was compiled from the literature to determine an osteogenic signature (Chen et al., 2012; Choi et al., 2010; Granéli et al., 2014; Harkness et al., 2011; Hoshiba et al., 2009; Liu et al., 2013; Miguez et al., 2014; Nora et al., 2012; Olivares-Navarrete et al., 2011). All RNA-seq analysis were performed with ≥2 biological replicates.

Immunohistochemistry, confocal imaging and quantitation

For harvesting the heart, the left ventricle was perfused with 5 mL PBS followed by 2 mL of 4% paraformaldehyde (PFA). The hearts were post fixed in 4% PFA for additional 4 hr and cryo-protected using 25% sucrose and embedded in OCT compound (Tissue-Tek). Immunofluorescent staining was performed on 7 μm frozen sections. For triple staining of calcium hydroxyapatite (HA) and osteogenic markers, sections were initially stained (according to manufacturer's instructions) with OsteoImage (Lonza, PA 1503, Walkersville, MD, USA), a fluorescent dye that stains hydroxyapatite. Sections were washed and blocked using 10% normal goat serum for 1 hr and then stained with primary antibodies against Runx2 (Novus biologicals, NBP1-77461), Osteocalcin (Abcam, ab 93876), Osterix (Santacruz, sc 22536-R), CD146 (Abcam, ab75769), NG2 (EMD Millipore, AB5320), ENPP1 (Abcam, ab40003), ALP (R&D Systems, AF2910), Osteopontin (Abcam, ab8448), Troponin (Santacruz, sc-8121) and CD31 (Abcam, ab7388) for overnight at 4°C. After washing three times with PBS, sections were incubated in secondary antibodies for 1ch followed by washing an additional three times with PBS. Finally, the sections were mounted in slow fade gold antifade reagent with DAPI (Life technologies, S36938). Labeled sections were imaged using a LSM 780 inverted Laser Scanning Confocal Microscope (Zeiss) or Digital Eclipse C1 Confocal Microscope System (Nikon). For each sample, eight independent images within 100μm radius of the calcified region were used for quantitative analysis. The images were merged using ImageJ software (NIH) and the total number of tdTomato cells expressing different osteogenic markers (double positive cells) was expressed as a fraction of the number of tdTomato cells present.

Confocal Raman Microscopy

Raman spectra were measured using a confocal Raman microscope (inVia Qontor) under 785 nm laser excitation at room temperature. The laser power used was ~50 mW. The grating used was 1200 l/mm, and the objective lens used was 20X with N.A. 0.4. Exposure time and the accumulation time for standard HA (Sigma, 574791) and CPPD (InvivoGen, tlrl-cppd) were 1 s and 60 times, respectively (Chen et al., 2009). For heart tissue Raman measurement, exposure time and the accumulation time were 1 s and 35 times, respectively. Raman data were analyzed using Renishaw WiRE 4.0 software.

Von Kossa and Masson's trichrome staining

Von Kossa staining on heart section was performed using Von Kossa staining reagent (Abcam, ab150687) as per manufacturer's instructions. Masson's trichrome staining was performed on heart sections using the reagent (Sigma, HT15-1KT) as per manufacturer's instructions (Ubil et al., 2014).

Alkaline Phosphatase activity and Phosphate assay

Injury and uninjured regions within the same heart were homogenized in ultrapure water (1mg tissue/ 50 uL water). Following homogenization the samples were placed into a 10kDa spin column (Thermo, 88513) at 14,000xg for 5 min. Alkaline Phosphatase activity was quantified by SensoLyte® pNPP Alkaline Phosphatase Assay Kit (Anaspec, AS-72146) and Phosphate by PiPer Phosphate Assay Kit (Invitrogen, MP22061).

Quantitative real-time PCR

RNA was isolated from cardiac fibroblasts at 3, 7, 14 and 21 days after the induction of differentiation and from control cells maintained in growth medium without differentiation factors. RNA isolation was performed using QIAGEN RNA Isolation Kit and reverse transcription using Reverse Transcription System (Promega, A3500). qPCR was performed using the SensiMix SYBR and Fluorescein Kit (Quantace, QT615) on an iQ5 thermal cycler (BioRad).

Flow cytometry analysis and sorting

Cultured cardiac fibroblasts were dissociated using accutase (Innovative Cell Technologies), stained in FACS buffer (0.1%BSA PBS) with APC-conjugated anti-Sca1 antibody (17-5981 -eBioscience) or PDGFRβ (17-1402, eBioscience), for 20cmin at 4°C. After washing with FACS buffer twice, stained cells were sorted in FACS Aria II (BD Biosciences). Similarly, flow cytometric analysis for cell surface markers were done using antibodies c-Kit APC (561074, BD Bioscience). For isolation of tdTomato labeled cardiac fibroblasts, cardiac fibroblasts isolated from non-transgenic mice were first run through the flow cytometer to establish gates. Next population of cardiac fibroblasts isolated from Col1a2-CreERT:R26R^{tdTomato} or FSP1Cre:R26R^{tdTomato} mice hearts were run through the same gates to identify tdTomato labeled cells. Similarly for other antigens analyzed on tdTomato labeled cells, unstained control cells were run first to establish gates followed by the cells stained with the primary antibody conjugated to the fluorophore.

Colony forming unit (CFU) assay

Sca1 positive and negative cells were sorted by flow cytometry and seeded in a 10 cm tissue culture dish at a density of 5X10^2 cells per dish for determination of colony forming unit capacity as described (Chong et al., 2011). The cells were maintained in growth medium for 10 days, then fixed in 2% paraformaldehyde for 30 min at 4°C, stained with 0.5% crystal violet (Fisher, C581-25,w/v in water) for 30 min at room temperature. Whole stained plates were scanned in an HP scanner, Microtek Scanmaker i800) at a resolution of 4200 pixels/inch and the number of colonies per plate were counted manually. Colony forming efficiency was expressed as a percentage of number of colonies formed per 5X10^2 cells plated. Representative images from three independent biological samples were shown in the figure.

Explant culture and Ectopic Bone formation Assay of cardiac fibroblasts

For explant culture, the mice subjected to cryo-injury were deeply anesthetized and perfused with 5 mL of HBSS (GIBCO). The calcified myocardial region was dissected out and diced into 2-3 mm pieces, and were placed in collagen coated (50μg/ml) tissue culture plates. Outgrowth cells were observed by day 1 and these cells were maintained in IMDM, 1X penicillin/streptomycin, 20% FBS for 5-7 days and were harvested for further experiments.

Assessment of osteogenic potential of cells from calcified and control cardiac fibroblasts were done using ectopic in vivo bone formation assay as described previously (Abdallah et al., 2008). Genetically labeled cardiac fibroblasts ($1x10^6$ cells resuspended in 100ul of IMDM, 1X penicillin/streptomycin, 10% FBS medium) from either explant cultures of calcified or from uninjured Collagen1a2-CreERT: $R26R^{tdTomato}$ mice, were loaded onto 40mg of wet hydroxyapatite and β-tri-calcium phosphate granules (Berkeley Advanced Biomaterials,Bio-02G) in a syringe and incubated at 37°C for 1 hr. Implants having 40mg of hydroxyapatite and β-tri-calcium phosphate granules without cells were served as control in each transplanted mouse. For ectopic implantation, mice were initially anaesthetized with 3% isoflurane, maintained at 2% isoflurane and three small longitudinal incision of about 1cm were made and through a blunt dissection, three subcutaneous pockets were fashioned on the dorsum of mice. 200ul of the prepared mixture with or without cells was placed in different subcutaneous sites in wild-type C3H mouse and surgical sites were finally closed by suturing.

In vivo micro PET/CT imaging

After subcutaneous implantations, mice underwent weekly ^{18}F-sodium fluoride (^{18}F-NaF) microPET/CT imaging (Inveon microPET, Siemens Medical Solutions USA Inc.; CrumpCAT microCT, Arion Chatziioannou lab, UCLA). ^{18}F-NaF was produced as previously described (Czernin et al., 2010). The CrumpCAT, a Crump Institute prototype microCT, acquired images under "high resolution" continuous mode using a 50 kVp, 200 μA X-ray source with a 45 degree cone angle and positioned at 13-15 cm from the isocenter. The camera is a flat panel CMOS detector with a CsI scintillator (1536 by 1944 pixels, pitch of 75 μm). Images were taken with 720 projections at 100 ms per projection, and reconstructed using the Feldkamp algorithm with a voxel size of 125 μm and calibrated for Hounsfield units.

Mice were injected with 100 μCi ^{18}F-NaF. After 60 min probe uptake time, mice were anesthetized with 2% isoflurane and placed in a dedicated heated imaging chamber. microPET images were acquired for 600 s, followed by 3D histogramming and reconstruction with a zoom factor of 2.1 using 3D-OSEM with 2 iterations followed by MAP with 18 iterations (beta = 0.1). This was followed by microCT imaging. Images were analyzed using AMIDE version 1.0.5 and OsiriX version 3.8 imaging software. microPET and microCT quantifications were performed separately using AMIDE by drawing individual 3D isocontours each originating at an implanted nodular region. Total new bone formation (microPET) and calcification (microCT) were determined by multiplying the mean ROI value (percent injected dose per milliliter for microPET; Hounsfield units for microCT) by the total volume of the ROI. Values were normalized to no-cells control.

Analysis of the extent of calcification by CT scanning following injection of ENPP1 inhibitors was confirmed by an independent observer analyzing the data in a blinded manner.

QUANTIFICATION AND STATISTICAL ANALYSIS

All data is presented as mean ± standard error of the mean (SEM). The value of n is mentioned in the figure/figure legends and always stands for separate biological replicates. Statistical analysis was performed using GraphPad software (Prizm) using Student's t- test (two tailed) and one-way ANOVA with Tukey's multiple comparison analysis as appropriate. A P value < 0.05 was considered statistically significant and individual p values are mentioned in the figure/figure legends.

DATA AND SOFTWARE AVAILABILITY

Data Resources

Raw data files for the RNA sequencing analysis have been deposited in the NCBI Gene Expression Omnibus under accession number GEO: GSE87836 and GEO: GSE87837.